CHAPTER 3

Modeling the Effects of Aerosols on Climate

Lead authors: **David Rind**, NASA GISS; **Mian Chin**, NASA GSFC; **Graham Feingold**, NOAA ESRL; **David G. Streets**, DOE ANL

Contributing authors: **Ralph A. Kahn**, NASA GSFC; **Stephen E. Schwartz**, DOE BNL; **Hongbin Yu**, NASA GSFC/UMBC

3.1. Introduction

The IPCC Fourth Assessment Report (AR4) (IPCC, 2007) concludes that man's influence on the warming climate is in the category of "very likely". This conclusion is based on, among other things, the ability of models to simulate the global and, to some extent, regional variations of temperature over the past 50 to 100 years. When anthropogenic effects are included, the simulations can reproduce the observed warming (primarily for the past 50 years); when they are not, the models do not get very much warming at all. In fact, all of the models runs for the IPCC AR4 assessment (more than 20 here) produce this distinctive result, driven by the greenhouse gas increases that have been observed to occur.

These results were produced in models whose global warming associated with a doubled CO_2 forcing of about 4 W m^{-2} was on average of an order of 3°C, hence translating this into a climate sensitivity (surface temperature change in response to atmospheric CO_2 change) of 0.75°C/Wm^{-2}. The determination of this value is crucial to predicting the future impact of increased greenhouse gases, and the credibility of this predicted value relies on the ability of these models to simulate the observed temperature changes over the past century. However, in producing the observed temperature trend in the past, the models made use of very uncertain aerosol forcing. The greenhouse gas change by itself produces warming in models that exceeds that observed by some 40% on average (IPCC, 2007). Cooling associated with aerosols reduces this warming to the observed level. Different climate models use differing aerosol forcings, both direct (aerosol scattering and absorption of short and longwave radiation) and indirect (aerosol effect on cloud cover reflectivity and lifetime), whose magnitudes vary markedly from one model to the next. Kiehl (2007) using nine of the IPCC (2007) AR4 climate models found that they had a factor of three forcing differences in the aerosol contribution for the 20th century. The differing aerosol forcing is the prime reason why models whose climate sensitivity varies by almost a factor of three can produce the observed trend. It was thus concluded that the uncertainty in IPCC (2007) anthropogenic climate simulations for the past century should really be much greater than stated (Schwartz et al., 2007; Kerr, 2007), since, in general, models with low/high sensitivity to greenhouse warming used weaker/stronger aerosol cooling to obtain the same temperature response (Kiehl, 2007). Had the situation been reversed and the low/high sensitivity models used strong/weak aerosol forcing, there would have been a greater divergence in model simulations of the past century.

Therefore, the fact that a model has accurately reproduced the global temperature change in the past does not imply that its future forecast is reliable. This state of affairs will remain until a

firmer estimate of radiative forcing (RF) by aerosols, in addition to that by greenhouse gases, is available.

Two different approaches are used to assess the aerosol effect on climate. "Forward modeling" studies incorporate different aerosol types and attempt to explicitly calculate the aerosol RF. From this approach, IPCC (2007) concluded that the best estimate of the global aerosol direct RF (compared with preindustrial times) is -0.5 (-0.9 to -0.1) W m^{-2} (see Figure 1.3, Chapter 1). The RF due to the cloud albedo or brightness effect (also referred to as first indirect or Twomey effect) is estimated to be -0.7 (-1.8 to -0.3) W m^{-2}. No estimate was specified for the effect associated with cloud lifetime. The total negative RF due to aerosols according to IPCC (2007) estimates (see Figure 1.3 in Chapter 1) is then -1.3 (-2.2 to -0.5) W m^{-2}. In comparison, the positive radiative forcing (RF) from greenhouse gases (including tropospheric ozone) is estimated to be +2.9 ± 0.3 W m^{-2}; hence tropospheric aerosols reduce the influence from greenhouse gases by about 45% (15-85%). This approach however inherits large uncertainties in aerosol amount, composition, and physical and optical properties in modeling of atmospheric aerosols. The consequences of these uncertainties are discussed in the next section.

The other method of calculating aerosol forcing is called the "inverse approach" – it is assumed that the observed climate change is primarily the result of the known climate forcing contributions. If one further assumes a particular climate sensitivity (or a range of sensitivities), one can determine what the total forcing had to be to produce the observed temperature change. The aerosol forcing is then deduced as a residual after subtraction of the greenhouse gas forcing along with other known forcings from the total value. Studies of this nature come up with aerosol forcing ranges of -0.6 to -1.7 W m^{-2} (Knutti et al., 2002, 2003; IPCC AR4 Chap.9); -0.4 to -1.6 W m^{-2} (Gregory et al., 2002); and -0.4 to -1.4 W m^{-2} (Stott et al., 2006). This approach however provides a bracket of the possible range of aerosol forcing without the assessment of current knowledge of the complexity of atmospheric aerosols.

This chapter reviews the current state of aerosol RF in the global models and assesses the uncertainties in these calculations. First representation of aerosols in the forward global chemistry and transport models and the diversity of the model simulated aerosol fields are discussed; then calculation of the aerosol direct and indirect effects in the climate models is reviewed; finally the impacts of aerosols on climate model simulations and their implications are assessed.

3.2. Modeling of Atmospheric Aerosols

The global aerosol modeling capability has developed rapidly in the past decade. In the late 1990s, there were only a few global models that were able to simulate one or two aerosol components, but now there are a few dozen global models that simulate a comprehensive suite of aerosols in the atmosphere. As introduced in Chapter 1, aerosols consist of a variety of species including dust, sea salt, sulfate, nitrate, and carbonaceous aerosols (black and organic carbon) produced from natural and man-made sources with a wide range of physical and optical properties. Because of the complexity of the processes and composition and highly inhomogeneous distributions of aerosols, accurately modeling atmospheric aerosols and their effects remain a challenge. Models have to take into account not only the aerosol and precursor emissions, but also the chemical transformation, transport, and removal processes (e.g. dry and wet depositions) to simulate the aerosol mass concentrations. Furthermore, aerosol particle size

can grow in the atmosphere because the ambient water vapor can condense on the aerosol particles. This "swelling" process, called hygroscopic growth, is most commonly parameterized in the models as a function of relative humidity.

3.2.1. Estimates of Emissions

Aerosols have various sources from natural and anthropogenic processes. Natural emissions include wind-blown mineral dust, aerosol and precursor gases from volcanic eruptions, natural wild fires, vegetation, and oceans. Anthropogenic sources include emissions from fossil fuel and biofuel combustion, industrial processes, agriculture practices, and human-induced biomass burning.

Following earlier attempts to quantify man-made primary emissions of aerosols (Turco et al., 1983; Penner et al., 1993) systematic work was undertaken in the late 1990s to calculate emissions of black carbon (BC) and organic carbon (OC), using fuel-use data and measured emission factors (Liousse et al., 1996; Cooke and Wilson, 1996; Cooke et al., 1999). The work was extended in greater detail and with improved attention to source-specific emission factors in Bond et al. (2004), which provides global inventories of BC and OC for the year 1996, with regional and source-category discrimination that includes contributions from industrial, transportation, residential solid-fuel combustion, vegetation and open biomass burning (forest fires, agricultural waste burning, etc.), and diesel vehicles.

Emissions from natural sources—which include wind-blown mineral dust, wildfires, sea salt, and volcanic eruptions—are less well quantified, mainly because of the difficulties of measuring emission rates in the field and the unpredictable nature of the events. Often, emissions must be inferred from ambient observations at some distance from the actual source. As an example, it was concluded (Lewis and Schwartz, 2004) that available information on size-dependent sea salt production rates could only provide order-of-magnitude estimates. The natural emissions in general can vary dramatically over space and time.

Aerosols can be produced from trace gases in the atmospheric via chemical reactions, and those aerosols are called *secondary* aerosols, as distinct from *primary* aerosols that are directly emitted to the atmosphere as aerosol particles. For example, most sulfate and nitrate aerosols are secondary aerosols that are formed from their precursor gases, sulfur dioxide (SO_2) and nitrogen oxides (NO and NO_2, collectively called NO_x), respectively. Those sources have been studied for many years and are relatively well known. By contrast, the sources of secondary organic aerosols (SOA) are poorly understood, including emissions of their precursor gases (called volatile organic compounds, VOC) from both natural and anthropogenic sources and the atmospheric production processes.

Globally, sea salt and mineral dust dominate the total aerosol mass emissions because of the large source areas and/or large particle sizes. However, sea salt and dust also have shorter atmospheric lifetimes because of their large particle size, and are radiatively less active than aerosols with small particle size, such as sulfate, nitrate, BC, and particulate organic matter (POM, which includes both carbon and non-carbon mass in the organic aerosol, see Glossary), most of which are anthropogenic in origin.

Because the anthropogenic aerosol RF is usually evaluated (e.g., by the IPCC) as the anthropogenic perturbation since the pre-industrial period, it is necessary to estimate the

historical emission trends, especially the emissions in the pre-industrial era. Compared to estimates of present-day emissions, estimates of historical emission have much larger uncertainties. Information for past years on the source types and strengths and even locations are difficult to obtain, so historical inventories from pre-industrial times to the present have to be based on limited knowledge and data. Several studies on historical emission inventories of BC and OC (e.g., Novakov et al., 2003; Ito and Penner 2005; Bond et al., 2007; Fernandes et al., 2007; Junker and Liousse, 2008), SO_2 (Stern, 2005), and various species (van Aardenne et al., 2001; Dentener et al., 2006) are available in the literature; there are some similarities and some differences among them, but the emission estimates for early times do not have the rigor of the studies for present-day emissions. One major conclusion from all these studies is that the growth of primary aerosol emissions in the 20th century was not nearly as rapid as the growth in CO_2 emissions. This is because in the late 19th and early 20th centuries, particle emissions such as BC and POM were relatively high due to the heavy use of biofuels and the lack of particulate controls on coal-burning facilities; however, as economic development continued, traditional biofuel use remained fairly constant and particulate emissions from coal burning were reduced by the application of technological controls (Bond et al., 2007). Thus, particle emissions in the 20th century did not grow as fast as CO_2 emissions, as the latter are roughly proportional to total fuel use—oil and gas included. Another challenge is estimating historical biomass burning emissions. A recent study suggested about a 40% increase in carbon emissions from biomass burning from the beginning to the end of last century (Mouillot et al., 2006), but it is difficult to verify.

As an example, **Table 3.1** shows estimated anthropogenic emissions of sulfur, BC and POM in the present day (year 2000) and pre-industrial time (1750) compiled by Dentener et al., 2006. These estimates have been used in the Aerosol Comparisons between Observations and Models (AeroCom) project (Experiment B, which uses the year 2000 emission; and Experiment PRE, which uses pre-industrial emissions), for simulating atmospheric aerosols and anthropogenic aerosol RF. The AeroCom results are discussed in Sections 3.2.2 and 3.3.

Table 3.1. Anthropogenic emissions of aerosols and precursors for 2000 and 1750. Adapted from Dentener et al., 2006.

Source	Species*	Emission[#] 2000 (Tg/yr)	Emission 1750 (Tg/yr)
Biomass burning	BC	3.1	1.03
	POM	34.7	12.8
	S	4.1	1.46
Biofuel	BC	1.6	0.39
	POM	9.1	1.56
	S	9.6	0.12
Fossil fuel	BC	3.0	
	POM	3.2	
	S	98.9	

[#]Data source for 2000 emission: biomass burning – Global Fire Emission Dataset (GFED); biofuel BC and POM – Speciated Pollutant Emission Wizard (SPEW); biofuel sulfur – International Institute for Applied System Analysis (IIASA); fossil fuel BC and POM – SPEW; fossil fuel sulfur – Emission Database for Global Atmospheric Research (EDGAR) and IIASA. Fossil fuel emission of sulfur (S) is the sum of emission from industry, power plants, and transportation listed in Dentener et al., 2006.

*S=sulfur, including SO_2 and particulate sulfate. Most emitted as SO_2, and 2.5% emitted as sulfate.

Projections of aerosol emissions into the future have been made, for example, in support of the IPCC Third Assessment Report (TAR) (IPCC, 2001). More recent forecasts of future BC and OC emissions based on future energy and fuel scenarios take care to incorporate the likely future effects of new technology deployment and environmental regulation (e.g., Streets et al., 2004; Rao et al., 2005). The expectation is that global emissions of carbonaceous aerosols (BC and OC) will likely remain flat or slightly decrease out to 2050. Prospective emissions

depend strongly on assumptions about future emission controls. The effect of such emissions on future aerosol composition is discussed in Synthesis and Assessment Product (SAP) 3.2.

3.2.2. Aerosol Mass Loading and Optical Depth

In the global models, aerosols are usually simulated in the successive steps of sources (emission and chemical formation), transport (from source location to other area), and removal processes (dry deposition, in which particles fall onto the surface, and wet deposition by rain) that control the aerosol lifetime. Collectively, emission, transport, and removal determine the amount (mass) of aerosols in the atmosphere.

Aerosol optical depth (AOD), which is a measure of solar or thermal radiation being attenuated by aerosol particles via scattering or absorption, can be related to the atmospheric aerosol mass loading as follows:

$$AOD = MEE \cdot M \tag{3.1}$$

where M is the aerosol mass loading per unit area (g m^{-2}), MEE is the mass extinction efficiency or specific extinction in unit of m^2 g^{-1}, which is

$$MEE = \frac{3Q_{ext}}{4\pi\rho r_{eff}} \cdot f \tag{3.2}$$

where Q_{ext} is the extinction coefficient (a function of particle size distribution and refractive index), r_{eff} is the aerosol particle effective radius, ρ is the aerosol particle density, and f is the ratio of ambient aerosol mass (wet) to dry aerosol mass M. Here, M is the result from model-simulated atmospheric processes and *MEE* embodies the aerosol physical (including microphysical) and optical properties. Since Q_{ext} varies with radiation wavelength, so do MEE and AOD. AOD is the quantity that is most commonly obtained from remote sensing measurements and is frequently used for model evaluation (see Chapter 2). AOD is also a key parameter determining aerosol radiative effects.

Here the results from the recent multiple-global-model studies by the AeroCom project are summarized, as they represent the current assessment of model-simulated atmospheric aerosol loading, optical properties, and RF for the present-day. AeroCom aims to document differences in global aerosol models and compare the model output to observations. Sixteen global models participated in the AeroCom Experiment A, for which every model used their own configuration, including their own choice of estimating emissions (Kinne et al., 2006; Textor et al., 2006). Five major aerosol types: sulfate, BC, POM, dust, and sea salt, were included in the experiments, although some models had additional aerosol species. Of those major aerosol types, dust and sea-salt are predominantly natural in origin, whereas sulfate, BC, and POM have major anthropogenic sources.

Table 3.2 summarizes the model results from the AeroCom-A for several key parameters: Sources (emission and chemical transformation), mass loading, lifetime, removal rates, MEE and AOD at a commonly used, mid-visible, wavelength of 550 nanometer (nm). These are the globally averaged values for the year 2000. Major features and conclusions are:

- Globally, aerosol source (in mass) is dominated by sea salt, followed by dust, sulfate, particulate organic matter, and black carbon. Over the non-desert land area, human activity is the major source of sulfate, black carbon, and organic aerosols.

- Aerosols are removed from the atmosphere by wet and dry deposition. Although sea salt dominates the emissions, it is quickly removed from the atmosphere because of its large particle size and near-surface distributions, thus having the shortest lifetime. The median lifetime of sea salt from the AeroCom-A models is less than half a day, whereas dust and sulfate have similar lifetimes of 4 days and BC and POM 6-7 days.

- Globally, small-particle-sized sulfate, BC, and POM make up a little over 10% of total aerosol mass in the atmosphere. However, they are mainly from anthropogenic activity, so the highest concentrations are in the most populated regions, where their effects on climate and air quality are major concerns.

- Sulfate and BC have their highest MEE at mid-visible wavelengths, whereas dust is lowest among the aerosol types modeled. That means for the same amount of aerosol mass, sulfate and BC are more effective at attenuating (scattering or absorbing) solar radiation than dust. This is why the sulfate AOD is about the same as dust AOD even though the atmospheric amount of sulfate mass is 10 times less than that of the dust.

- There are large differences, or diversities, among the models for all the parameters listed in Table 3.2. The largest model diversity, shown as the % standard deviation from the all-model-mean and the range (minimum and maximum values) in Table 3.2, is in sea salt emission and removal; this is mainly associated with the differences in particle size range and source parameterizations in each model. The diversity of sea salt atmospheric loading however is much smaller than that of sources or sinks, because the largest particles have the shortest lifetimes even though they comprise the largest fraction of emitted and deposited mass.

- Among the key parameters compared in Table 3.2, the models agree best for simulated total AOD – the % of standard deviation from the model mean is 18%, with the extreme values just a factor of 2 apart. The median value of the multi-model simulated global annual mean total AOD, 0.127, is also in agreement with the global mean values from recent satellite measurements. However, despite the general agreement in total AOD, there are significant diversities at the individual component level for aerosol optical thickness, mass loading, and mass extinction efficiency. This indicates that uncertainties in assessing aerosol climate forcing are still large, and they depend not only on total AOD but also on aerosol absorption and scattering direction (see Glossary), both of which are determined by aerosol physical and optical properties. In addition, even with large differences in mass loading and MEE among different models, these terms could compensate for each other (eq. 3.1) to produce similar AOD. This is illustrated in **Figure 3.1**. For example, model LO and LS have quite different mass loading (44 and 74 mg m^{-2}, respectively), especially for dust and sea salt amount, but they produce nearly identical total AOD (0.127 and 0.128, respectively).

- Because of the large spatial and temporal variations of aerosol distributions, regional and seasonal diversities are even larger than the diversity for global annual means.

Table 3.2. Summary of statistics of AeroCom Experiment A results from 16 global models. Data from Textor et al. (2006) and Kinne et al. (2006), and AeroCom website (http://nansen.ipsl.jussieu.fr/AEROCOM/data.html).

	Mean	Median	Range	Stddev /mean*
Sources (Tg yr^{-1}):				
Sulfate	179	186	98 – 232	22%
Black carbon	11.9	11.3	7.8 – 19.4	23%
Organic matter	96.6	96.0	53 – 138	26%
Dust	1840	1640	672 – 4040	49%
Sea salt	16600	6280	2180 – 121000	199%
Removal rate (day^{-1}):				
Sulfate	0.25	0.24	0.19 – 0.39	18%
Black carbon	0.15	0.15	0.066 – 0.19	21%
Organic matter	0.16	0.16	0.09 – 0.23	24%
Dust	0.31	0.25	0.14 – 0.79	62%
Sea salt	5.07	2.50	0.95 – 35.0	188%
Lifetime (day):				
Sulfate	4.12	4.13	2.6 – 5.4	18%
Black carbon	7.12	6.54	5.3 – 15	33%
Organic matter	6.54	6.16	4.3 – 11	27%
Dust	4.14	4.04	1.3 – 7.0	43%
Sea salt	0.48	0.41	0.03 – 1.1	58%
Mass loading (Tg):				
Sulfate	1.99	1.98	0.92 – 2.70	25%
Black carbon	0.24	0.21	0.046 – 0.51	42%
Organic matter	1.70	1.76	0.46 – 2.56	27%
Dust	19.2	20.5	4.5 – 29.5	40%
Sea salt	7.52	6.37	2.5 – 13.2	54%
MEE at 550 nm (m^2 g^{-1}):				
Sulfate	11.3	9.5	4.2 – 28.3	56%
Black carbon	9.4	9.2	5.3 – 18.9	36%
Organic matter	5.7	5.7	3.7 – 9.1	26%
Dust	0.99	0.95	0.46 – 2.05	45%
Sea salt	3.0	3.1	0.97 – 7.5	55%
AOD at 550 nm:				
Sulfate	0.035	0.034	0.015 – 0.051	33%
Black carbon	0.004	0.004	0.002 – 0.009	46%
Organic matter	0.018	0.019	0.006 – 0.030	36%
Dust	0.032	0.033	0.012 – 0.054	44%
Sea salt	0.033	0.030	0.02 – 0.067	42%
Total AOT at 550 nm	0.124	0.127	0.065 – 0.151	18%

*Stddev/mean was used as the term “diversity” in Textor et al., 2006.

To further isolate the impact of the differences in emissions on the diversity of simulated aerosol mass loading, identical emissions for aerosols and their precursor were used in the AeroCom Experiment B exercise in which 12 of the 16 AeroCom-A models participated (Textor et al., 2007). The comparison of the results and diversity between AeroCom-A and -B for the same models showed that using harmonized emissions does not significantly reduce model diversity for the simulated global mass and AOD fields, indicating that the differences in atmospheric processes, such as transport, removal, chemistry, and aerosol microphysics, play more important roles than emission in creating diversity among the models. This outcome is somewhat different

from another recent study, in which the differences in calculated clear-sky aerosol RF between two models (a regional model STEM and a global model MOZART) were attributed mostly to the differences in emissions (Bates et al., 2006), although the conclusion was based on only two model simulations for a few focused regions. It is highly recommended from the outcome of AeroCom-A and -B that, although more detailed evaluation for each individual process is needed, multi-model ensemble results, e.g., median values of multi-model output variables, should be used to estimate aerosol RF, due to their greater robustness, relative to individual models, when compared to observations (Textor et al., 2006, 2007; Schulz et al., 2006).

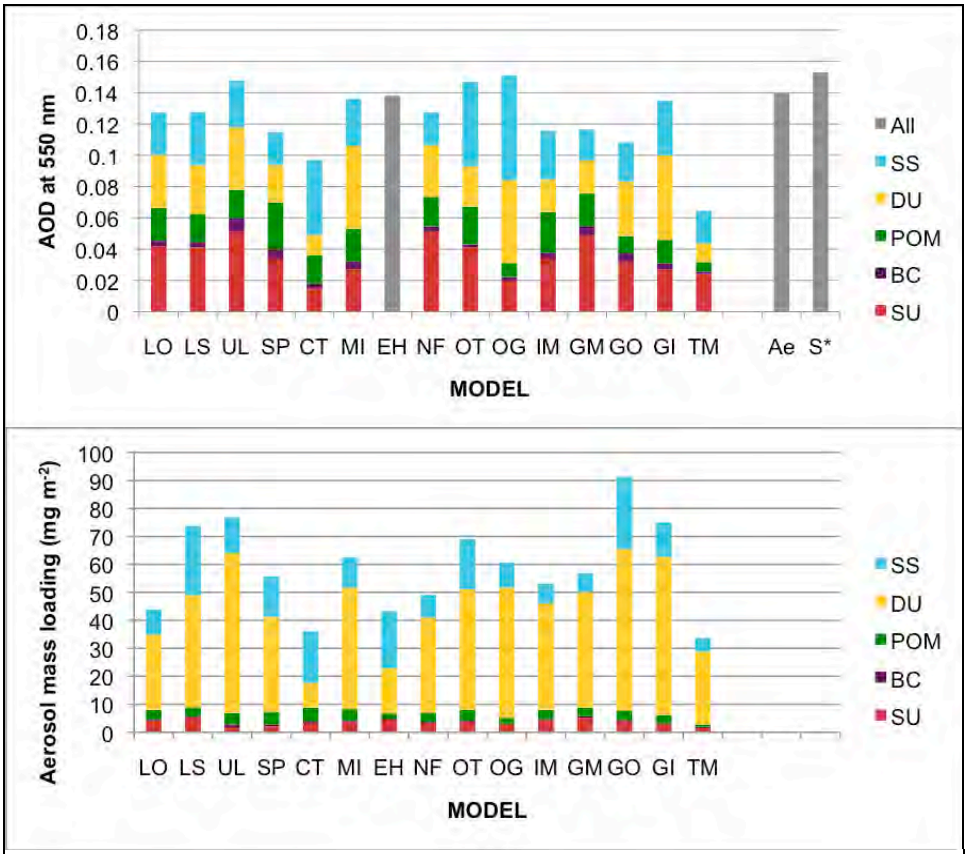

Figure 3.1. Global annual averaged AOD (upper panel) aerosol mass loading (lower panel) with their components simulated by 15 models in AeroCom-A (exclude1 model which only reported mass). SU=sulfate, BC=black carbon, POM=particulate organic carbon, DU=dust, SS=sea salt. Model abbreviations: LO=LOA (Lille, Fra), LS=LSCE (Paris, Fra), UL=ULAQ (L'Aquila, Ita), SP=SPRINTARS (Kyushu, Jap), CT=ARQM (Toronto, Can), MI=MIRAGE (Richland, USA), EH=ECHAM5 (MPI-Hamburg, Ger), NF=CCM-Match (NCAR-Boulder, USA), OT=Oslo-CTM (Oslo, Nor), OG=OLSO-GCM (Oslo, Nor) [prescribed background for DU and SS], IM=IMPACT (Michigan, USA), GM=GFDL-Mozart (Princeton, NJ, USA), GO=GOCART (NASA-GSFC, Washington DC, USA), GI=GISS (NASA-GISS, New York, USA), TM=TM5 (Utrecht, Net). Also shown in upper panel are the averaged observation data from AERONET (Ae) and satellite composite (S*). See Kinne et al. (2006) for details. Figure produced from data in Kinne et al. (2006).

3.3. Calculating Aerosol Direct Radiative Forcing

The three parameters that define the aerosol direct RF are the AOD, the single scattering albedo (SSA), and the asymmetry factor (g), all of which are wavelength dependent. AOD is indicative of how much aerosol exists in the column, SSA is the fraction of radiation being scattered versus the total attenuation (scattered and absorbed), and the g relates to the direction of scattering that is related to the size of the particles (see Chapter 1). An indication of the particle size is provided by another parameter, the Ångström exponent (Å), which is a measure of differences of AOD at different wavelengths. For typical tropospheric aerosols, Å tends to be inversely dependent on particle size; larger values of Å are generally associated with smaller aerosols particles. These parameters are further related; for example, for a given composition, the ability of a particle to scatter radiation decreases more rapidly with decreasing size than does its ability to absorb, so at a given wavelength varying Å can change SSA. Note that AOD, SSA, g, Å, and all the other parameters in eq. 3.1 and 3.2 vary with space and time due to variations of both aerosol composition and relative humidity, which influence these characteristics.

In the recent AeroCom project, aerosol direct RF for the solar spectral wavelengths (or shortwave) was assessed based on the 9 models that participated in both Experiment B and PRE in which identical, prescribed emissions for present (year 2000) and pre-industrial time (year 1750) listed in Table 3.1 were used across the models (Schulz et al., 2006). The anthropogenic direct RF was obtained by subtracting AeroCom-PRE from AeroCom-B simulated results. Because dust and sea salt are predominantly from natural sources, they were not included in the anthropogenic RF assessment although the land use practice can contribute to dust emissions as "anthropogenic". Other aerosols that were not considered in the AeroCom forcing assessment were natural sulfate (e.g. from volcanoes or ocean) and POM (e.g. from biogenic hydrocarbon oxidation), as well as nitrate. The aerosol direct forcing in the AeroCom assessment thus comprises three major anthropogenic aerosol components sulfate, BC, and POM.

The IPCC AR4 (IPCC, 2007) assessed anthropogenic aerosol RF based on the model results published after the IPCC TAR in 2001, including those from the AeroCom study discussed above. These results (adopted from IPCC AR4) are shown in **Table 3.3** for sulfate and **Table 3.4** for carbonaceous aerosols (BC and POM), respectively. All values listed in Table 3.3 and 3.4 refer to anthropogenic perturbation, i.e. excluding the natural fraction of these aerosols. In addition to the mass burden, MEE, and AOD, Table 3.3 and 3.4 also list the "normalized forcing", also known as "forcing efficiency", one for the forcing per unit AOD, and the other the forcing per gram of aerosol mass (dry). For some models, aerosols are externally mixed, that is, each aerosol particle contains only one aerosol type such as sulfate, whereas other models allow aerosols to mix internally to different degrees, that is, each aerosol particle can have more than one component, such as black carbon coated with sulfate. For models with internal mixing of aerosols, the component values for AOD, MEE, and forcing were extracted (Schulz et al., 2006).

Considerable variation exists among these models for all quantities in Table 3.3 and 3.4. The RF for all the components varies by a factor of 6 or more: Sulfate from 0.16 to 0.96 W m^{-2}, POM from -0.06 to -0.34 W m^{-2}, and BC from +0.08 to +0.61 W m^{-2}, with the standard deviation in the range of 30 to 40% of the ensemble mean. It should be noted that although BC has the lowest mass loading and AOD, it is the only aerosol species that absorbs strongly, thus causing positive

forcing to warm the atmosphere, in contrast to other aerosols that impose negative forcing that cools the atmosphere. As a result, the net anthropogenic aerosol forcing as a whole becomes more negative. The global average anthropogenic aerosol direct RF at the top of the atmosphere (TOA) from the models, together with observation-based estimates (see Chapter 2), is presented in **Figure 3.2**. Note the wide range for forcing in Figure 3.2. The comparison with observation-based estimates shows that the model estimated forcing is in general lower, partially because the forcing value from the model is the difference between present-day and pre-industrial time, whereas the observation-derived quantity is the difference between an atmosphere with and without anthropogenic aerosols, so the "background" value that is subtracted from the total forcing is higher in the models.

Table 3.3. Sulfate mass loading, AOT at 550 nm, shortwave radiative forcing at the top of the atmosphere, and normalized forcing with respect to AOT and mass. All values refer to anthropogenic perturbation. Adapted from IPCC AR4 (2007) and Schulz et al. (2006).

Model	Mass load (mg m^{-2})	MEE (m^2 g^{-1})	AOD at 0.55 μm	TOA Forcing (W m^{-2})	Forcing/ AOD (W m^{-2})	Forcing/ mass (W g^{-1})
Published since IPCC 2001						
A CCM3	2.23			-0.56		-251
B GEOSCHEM	1.53	11.8	0.018	-0.33	-18	-216
C GISS	3.30	6.7	0.022	-0.65	-30	-197
D GISS	3.27			-0.96		-294
E GISS*	2.12			-0.57		-269
F SPRINTARS	1.55	9.7	0.015	-0.21		-135
G LMD	2.76			-0.42		-152
H LOA	3.03	9.9	0.03	-0.41	-14	-135
I GATORG	3.06			-0.32		-105
J PNNL	5.50	7.6	0.042	-0.44	-10	-80
K UIO-CTM	1.79	10.6	0.019	-0.37	-19	-207
L UIO-GCM	2.28			-0.29		-127
AeroCom: Identical emissions used for year 2000 and 1750						
M UMI	2.64	7.6	0.02	-0.58	-29	-220
N UIO-CTM	1.70	11.2	0.019	-0.36	-19	-212
O LOA	3.64	9.6	0.035	-0.49	-14	-135
P LSCE	3.01	7.6	0.023	-0.42	-18	-140
Q ECHAM5-HAM	2.47	6.5	0.016	-0.46	-29	-186
R GISS**	1.34	4.5	0.006	-0.19	-32	-142
S UIO-GCM	1.72	7.0	0.012	-0.25	-21	-145
T SPRINTARS	1.19	10.9	0.013	-0.16	-12	-134
U ULAQ	1.62	12.3	0.02	-0.22	-11	-136
Average A-L	**2.70**	**9.4**	**0.024**	**-0.46**	**-18**	**-181**
Average M-U	**2.15**	**8.6**	**0.018**	**-0.35**	**-21**	**-161**
Minimum A-U	**1.19**	**4.5**	**0.006**	**-0.96**	**-32**	**-294**
Maximum A-U	**5.50**	**12.3**	**0.042**	**-0.16**	**-10**	**-80**
Std dev A-L	**1.09**	**1.9**	**0.010**	**0.202**	**7**	**68**
Std dev M-U	**0.83**	**2.6**	**0.008**	**0.149**	**8**	**35**
%Stddev/avg A-L	**40%**	**20%**	**41%**	**44%**	**38%**	**38%**
%Stddev/avg M-U	**39%**	**30%**	**45%**	**43%**	**37%**	**22%**

Model abbreviations: CCM3=Community Climate Model; GEOSCHEM= Goddard Earth Observing System-Chemistry; GISS=Goddard Institute for Space Studies; SPRINTARS=Spectral Radiation-Transport Model for Aerosol Species; LMD=Laboratoire de Meteorologie Dynamique; LOA=Laboratoire d'Optique Atmospherique; GATORG=Gas, Aerosol Transport and General circulation model; PNNL=Pacific Northwest National Laboratory; UIO-CTM=Univeristy of Oslo CTM; UIO-GCM=University of Oslo GCM; UMI=University of Michigan; LSCE=Laboratoire des Sciences du Climat et de l'Enviornment; ECHAMS5-HAM=European Centre Hamburg with Hamburg Aerosol Module; ULAQ=University of lL'Aquila.

Table 3.4. Particulate organic matter (POM) and black carbon (BC) mass loading, AOD at 550 nm, shortwave radiative forcing at the top of the atmosphere, and normalized forcing with respect to AOD and mass. All values refer to anthropogenic perturbation. Based on IPCC AR4 (2007) and Schulz et al. (2006).

	POM						BC					
MODEL	**Mass load (mg m^{-2})**	**Mass ext. eff. (m^2 g^{-1})**	**AOD at 550 nm**	**TOA Forcing (W m^{-2})**	**Forcing/ AOD (W m^{-2})**	**Forcing /mass (W g^{-1})**	**Mass load (mg m^{-2})**	**Mass ext. eff. (m^2 g^{-1})**	**AOD at 550 nm x1000**	**TOA Forcing (W m^{-2})**	**Forcing/ AOD (W m^{-2})**	**Forcing/ mass (W g^{-1})**
Published since IPCC 2001												
A SPRINTARS				-0.24		-107				0.36		
B LOA	2.33	6.9	0.016	-0.25	-16	-140	0.37			0.55		
C GISS	1.86	9.1	0.017	-0.26	-15	-161	0.29			0.61		
D GISS	1.86	8.1	0.015	-0.30	-20	-75	0.29			0.35		
E GISS*	2.39			-0.18		-92	0.39			0.50		
F GISS	2.49			-0.23		-101	0.43			0.53		
G SPRINTARS	2.67	10.9	0.029	-0.27	-9	-23	0.53			0.42		
H GATORG	2.56			-0.06		-112	0.39			0.55		
I MOZGN	3.03	5.9	0.018	-0.34	-19							
J CCM							0.33			0.34		
K UIO-GCM							0.30			0.19		
AeroCom: Identical emissions for year 2000 & 1750												
L UMI	1.16	5.2	0.0060	-0.23	-38	-198	0.19	6.8	1.29	0.25	194	1316
M UIO-CTM	1.12	5.2	0.0058	-0.16	-28	-143	0.19	7.1	1.34	0.22	164	1158
N LOA	1.41	6.0	0.0085	-0.16	-19	-113	0.25	7.9	1.98	0.32	162	1280
O LSCE	1.50	5.3	0.0079	-0.17	-22	-113	0.25	4.4	1.11	0.30	270	1200
P ECHAM5-HAM	1.00	7.7	0.0077	-0.10	-13	-100	0.16	7.7	1.23	0.20	163	1250
Q GISS**	1.22	4.9	0.0060	-0.14	-23	-115	0.24	7.6	1.83	0.22	120	917
R UIO-GCM	0.88	5.2	0.0046	-0.06	-13	-68	0.19	10.3	1.95	0.36	185	1895
S SPRINTARS	1.84	10.9	0.0200	-0.10	-5	-54	0.37	9.5	3.50	0.32	91	865
T ULAQ	1.71	4.4	0.0075	-0.09	-12	-53	0.38	7.6	2.90	0.08	28	211
Average A-K	**2.40**	**8.2**	**0.019**	**-0.24**	**-16**	**-102**	**0.37**	**--**	**--**	**0.44**	**--**	**1242**
Average L-T	**1.32**	**6.1**	**0.008**	**-0.13**	**-19**	**-106**	**0.25**	**7.7**	**1.90**	**0.25**	**153**	**1121**
Minimum A-T	**0.88**	**4.4**	**0.005**	**-0.34**	**-38**	**-198**	**0.16**	**4.4**	**1.11**	**0.08**	**28**	**211**
Maximum A-T	**3.03**	**10.9**	**0.029**	**-0.06**	**-5**	**-23**	**0.53**	**10.3**	**3.50**	**0.61**	**270**	**2103**
Std dev A-K	**0.39**	**1.7**	**0.006**	**0.09**	**4**	**41**	**0.08**	**--**	**--**	**0.06**	**--**	**384**
Std dev L-T	**0.32**	**2.0**	**0.005**	**0.05**	**10**	**46**	**0.08**	**1.6**	**0.82**	**0.09**	**68**	**450**
%Stddev/avg A-K	**16%**	**21%**	**30%**	**36%**	**26%**	**41%**	**22%**	**--**	**--**	**23%**	**--**	**31%**
%Stddev/avg L-T	**25%**	**33%**	**56%**	**39%**	**52%**	**43%**	**32%**	**21%**	**43%**	**34%**	**45%**	**40%**

The discussion so far has dealt with global average values. The geographic distributions of multi-model aerosol direct RF has been evaluated among the AeroCom models, which are shown in **Figure 3.3** for total and anthropogenic AOD at 550 nm and anthropogenic aerosol RF at TOA, within the atmospheric column, and at the surface. Globally, anthropogenic AOD is about 25% of total AOD (Figure 3.3a and b) but is more concentrated over polluted regions in Asia, Europe, and North America and biomass burning regions in tropical southern Africa and South America. At TOA, anthropogenic aerosol causes negative forcing over mid-latitude continents and oceans with the most negative values (-1 to -2 W m^{-2}) over polluted regions (Figure 3.3c). Although anthropogenic aerosol has a cooling effect at the surface with surface forcing values down to -10

W m^{-2} over China, India, and tropical Africa (Figure 3.3e), it warms the atmospheric column with the largest effects again over the polluted and biomass burning regions. This heating effect will change the atmospheric circulation and can affect the weather and precipitation (e.g., Kim et al., 2006).

Basic conclusions from forward modeling of aerosol direct RF are:

- The most recent estimate of all-sky shortwave aerosol direct RF at TOA from anthropogenic sulfate, BC, and POM (mostly from fossil fuel/biofuel combustion and biomass burning) is -0.22±0.18 W m^{-2} averaged globally, exerting a net cooling effect. This value would represent the low-end of the forcing magnitude, since some potentially significant anthropogenic aerosols, such as nitrate and dust from human activities are not included because of their highly uncertain sources and processes. IPCC AR4 had adjusted the total anthropogenic aerosol direct RF to -0.5±0.4 W m^{-2} by adding estimated anthropogenic nitrate and dust forcing values based on limited modeling studies and by considering the observation-based estimates (see Chapter 2).

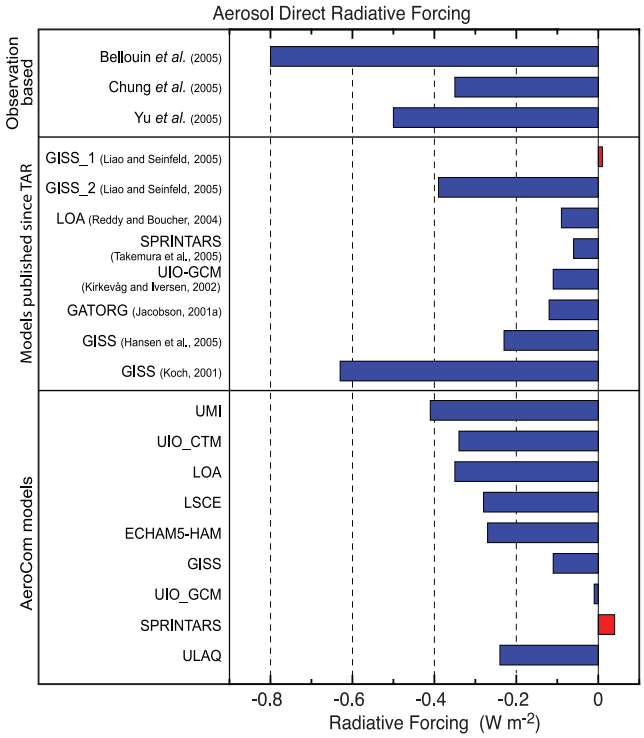

Figure 3.2. Aerosol direct radiative forcing in various climate and aerosol models. Observed values are shown in the top section. From IPCC (2007).

- Both sulfate and POM causes negative forcing whereas BC causes positive forcing because of its highly absorbing nature. Although BC comprises only a small fraction of anthropogenic aerosol mass load and AOD, its forcing efficiency (with respect to either AOD or mass) is an order of magnitude stronger than sulfate and POM, so its positive shortwave forcing largely offsets the negative forcing from sulfate and POM. This points out the importance of improving the model ability to simulate each individual aerosol components more accurately, especially black carbon. Separately, it is estimated from recent model studies that anthropogenic sulfate, POM, and BC forcings at TOA are -0.4, -0.18, +0.35 W m^{-2}, respectively. The anthropogenic nitrate and dust forcings are estimated at -0.1 W m^{-2} for each, with uncertainties exceeds 100% (IPCC AR4, 2007).

- In contrast to long-lived greenhouse gases, anthropogenic aerosol RF exhibits significant regional and seasonal variations. The forcing magnitude is the largest over the industrial and biomass burning source regions, where the magnitude of the negative aerosol forcing can be of the same magnitude or even stronger than that of positive greenhouse gas forcing.

- There is a large spread of model-calculated aerosol RF even in the global annual averaged values. The AeroCom study shows that the model diversity at some locations (mostly East

Asia and African biomass burning regions) can reach ±3 W m^{-2}, which is an order of magnitude above the global averaged forcing value of -0.22 W m^{-2}. The large diversity reflects the low level of current understanding of aerosol radiative forcing, which is compounded by uncertainties in emissions, transport, transformation, removal, particle size, and optical and microphysical (including hygroscopic) properties.

- In spite of the relatively small value of total anthropogenic aerosol forcing at TOA, the surface forcing and atmospheric column forcing values are considerably larger but opposite in sign: -1 to -2 W m^{-2} at the surface and +0.8 to +2 W m^{-2} in the atmosphere. Anthropogenic aerosols thus cool the surface but heat the atmosphere, on average. Regionally, the atmospheric heating can reach annually averaged values exceeding 5 W m^{-2} (Figure 3.3d). These regional effects and the negative surface forcing are expected to exert an important effect on climate through alteration of the hydrological cycle.

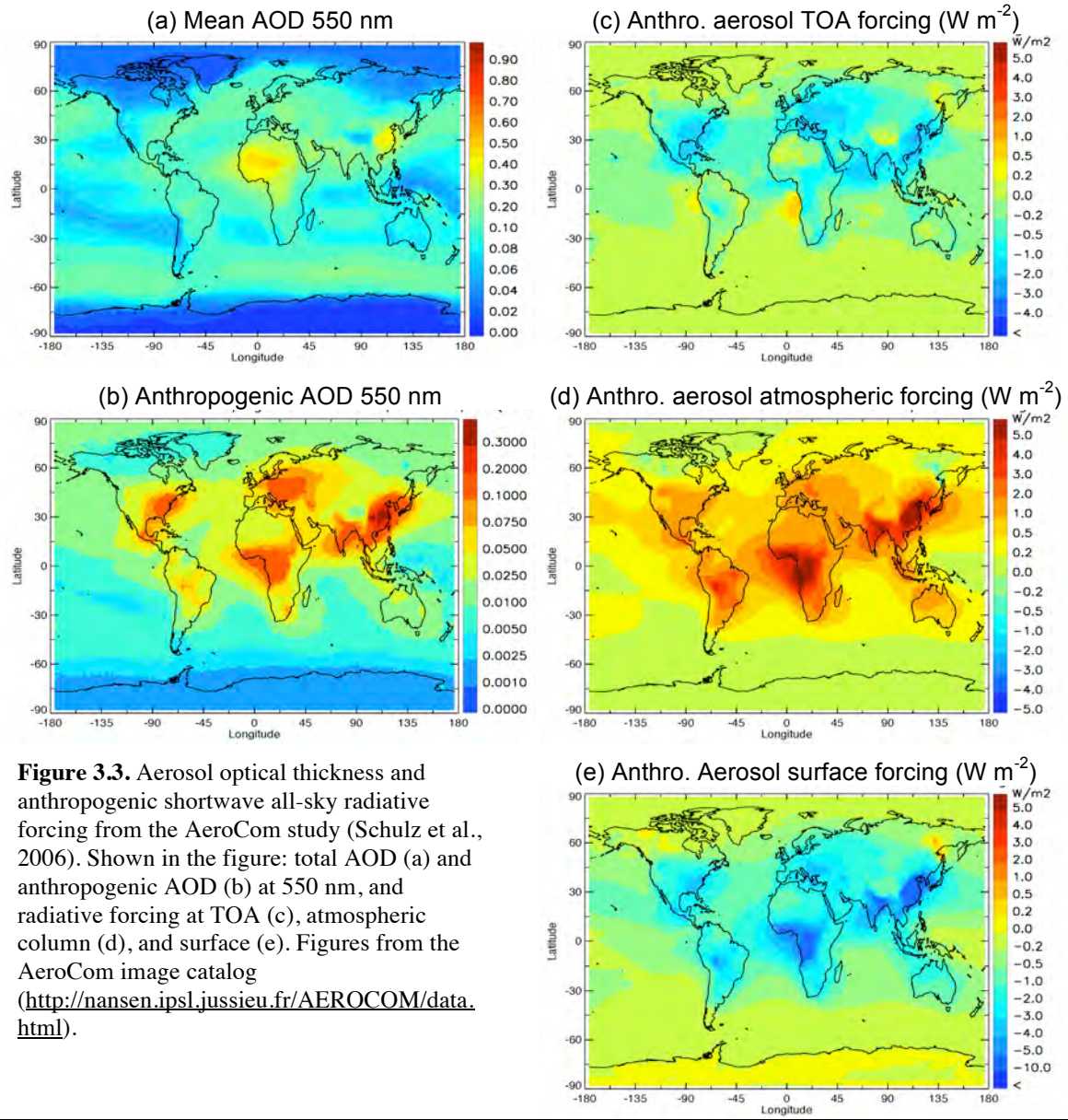

Figure 3.3. Aerosol optical thickness and anthropogenic shortwave all-sky radiative forcing from the AeroCom study (Schulz et al., 2006). Shown in the figure: total AOD (a) and anthropogenic AOD (b) at 550 nm, and radiative forcing at TOA (c), atmospheric column (d), and surface (e). Figures from the AeroCom image catalog (http://nansen.ipsl.jussieu.fr/AEROCOM/data.html).

3.4. Calculating Aerosol Indirect Forcing

3.4.1. Aerosol Effects on Clouds

A subset of the aerosol particles can act as cloud condensation nuclei (CCN) and/or ice nuclei (IN). Increases in aerosol particle concentrations, therefore, may increase the ambient concentrations of CCN and IN, affecting cloud properties. For a fixed cloud liquid water content, a CCN increase will lead to more cloud droplets so that the cloud droplet size will decrease. That effect leads to brighter clouds, the enhanced albedo then being referred to as the "cloud albedo effect" (Twomey, 1977), also known as the first indirect effect. If the droplet size is smaller, it may take longer to rainout, leading to an increase in cloud lifetime, hence the "cloud lifetime" effect (Albrecht, 1989), also called the second indirect effect. Approximately one-third of the models used for the IPCC 20th century climate change simulations incorporated an aerosol indirect effect, generally (though not exclusively) considered only with sulfates.

Shown in **Figure 3.4** are results from published model studies indicating the different RF values from the cloud albedo effect. The cloud albedo effect ranges from -0.22 to -1.85 W m^{-2}; the lowest estimates are from simulations that constrained representation of aerosol effects on clouds with satellite measurements of drop size vs. aerosol index. In view of the difficulty of quantifying this effect remotely (discussed later), it is not clear whether this constraint provides an improved estimate. The estimate in the IPCC AR4 ranges from +0.4 to -1.1 W m^{-2}, with a "best-guess" estimate of -0.7 W m^{-2}.

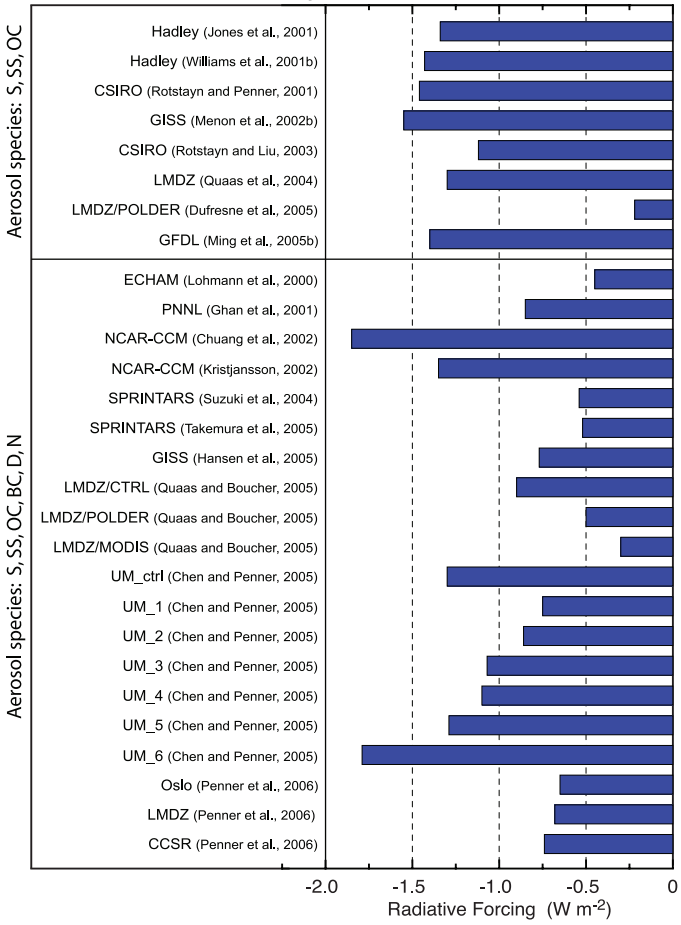

Fig. 3.4. Radiative forcing from the cloud albedo effect (1st aerosol indirect effect) in the global climate models used in IPCC 2007 (IPCC Fig. 2.14). For additional model designations and references, see IPCC 2007, chapter 2. Species included in the lower part of the panel include sulfate, sea salt, organic and black carbon, dust and nitrates; in the top panel only sulfate, sea salt and organic carbon.

The representation of cloud effects in GCMs is considered below. However, it is becoming increasingly clear from studies based on high resolution simulations of aerosol-cloud interactions that there is a great deal of complexity that is unresolved in climate models. This point is examined again in section 3.4.4.

Most models did not incorporate the "cloud lifetime effect". Hansen et al. (2005) compared this latter influence (in the form of time-averaged cloud area or cloud cover increase) with the cloud albedo effect. In contrast to the discussion in IPCC (2007), they argue

that the cloud cover effect is more likely to be the dominant one, as suggested both by cloud-resolving model studies (Ackerman et al., 2004) and satellite observations (Kaufman et al., 2005c). The cloud albedo effect may be partly offset by reduced cloud thickness accompanying aerosol pollutants, producing a meteorological (cloud) rather than aerosol effect (see the discussion in Lohmann and Feichter, 2005). (The distinction between meteorological feedback and aerosol forcing can become quite opaque; as noted earlier, the term feedback is restricted here to those processes that are responding to a change in temperature.) Nevertheless, both aerosol indirect effects were utilized in the GISS model, with the second indirect effect calculated by relating cloud cover to the aerosol number concentration, which in turn is a function of sulfate, nitrate, black carbon and organic carbon concentration. Only the low altitude cloud influence was modeled, principally because there are greater aerosol concentrations at low levels, and because low clouds currently exert greater cloud RF. The aerosol influence on high altitude clouds, associated with IN changes, is a relatively unexplored area for models and as well for process-level understanding.

Hansen et al. (2005) used coefficients to normalize the cooling from aerosol indirect effects to between -0.75 and -1 W m^{-2}, based on comparisons of modeled and observed changes in the diurnal temperature range as well as some satellite observations. The response of the GISS model to the direct and two indirect effects is shown in **Figure 3.5**. As parameterized, the cloud lifetime effect produced somewhat greater negative RF (cooling), but this was the result of the coefficients chosen. Geographically, it appears that the "cloud cover" effect produced slightly more cooling in the Southern Hemisphere than did the "cloud albedo" response, with the reverse being true in the Northern Hemisphere (differences on the order of a few tenths °C).

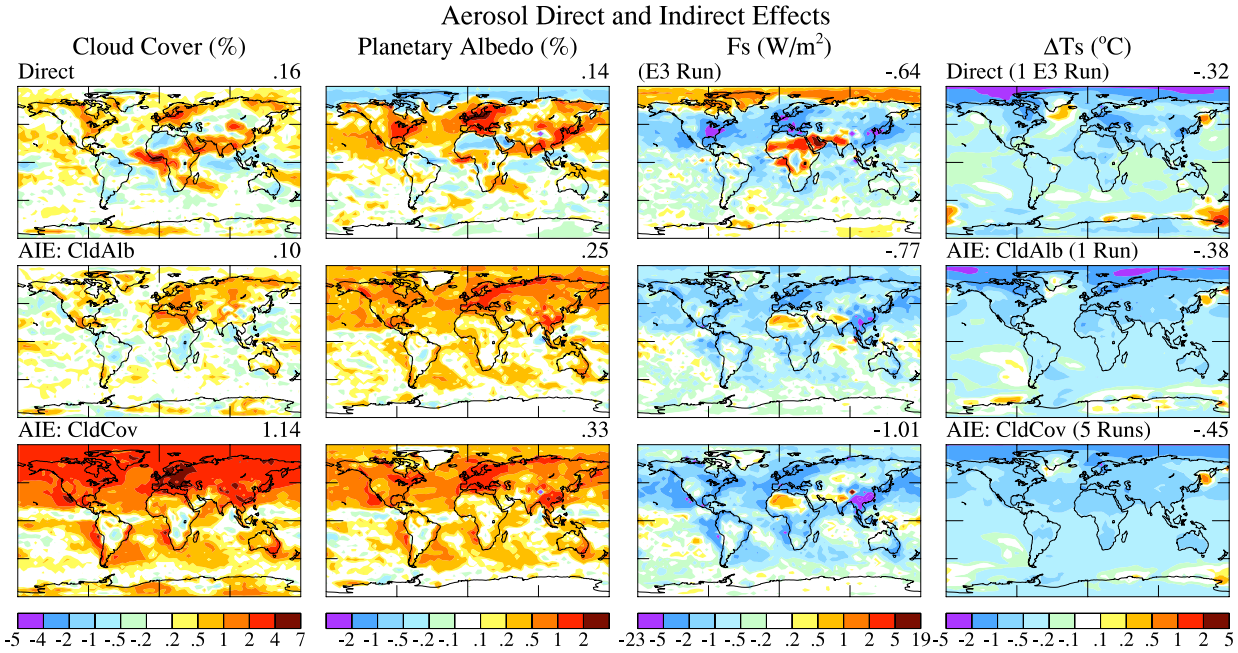

Fig. 3.5. Anthropogenic impact on cloud cover, planetary albedo, radiative flux at the surface (while holding sea surface temperatures and sea ice fixed) and surface air temperature change from the direct aerosol forcing (top row), the 1st indirect effect (second row) and the second indirect effect (third row). The temperature change is calculated from years 81-120 of a coupled atmosphere simulation with the GISS model. From Hansen et al., (2005).

3.4.2. Model Experiments

There are many different factors that can explain the large divergence of indirect effects in models (Fig. 3.4). To explore this in more depth, Penner et al. (2006) used three general circulation models to analyze the differences between models for the first indirect effect, as well as a combined first plus second indirect effect. The models all had different cloud and/or convection parameterizations.

In the first experiment, the monthly average aerosol mass and size distribution of, effectively, sulfate aerosol were prescribed, and all models followed the same prescription for parameterizing the cloud droplet number concentration (CDNC) as a function of aerosol concentration. In that sense, the only difference among the models was their separate cloud formation and radiation schemes. The different models all produced similar droplet effective radii, and therefore shortwave cloud forcing, and change in net outgoing whole sky radiation between pre-industrial times and the present. Hence the first indirect effect was not a strong function of the cloud or radiation scheme. The results for this and the following experiments are presented in **Figure 3.6**, where the experimental results are shown sequentially from left to right for the whole sky effect, and in **Table 3.5** for the clear-sky and cloud forcing response as well.

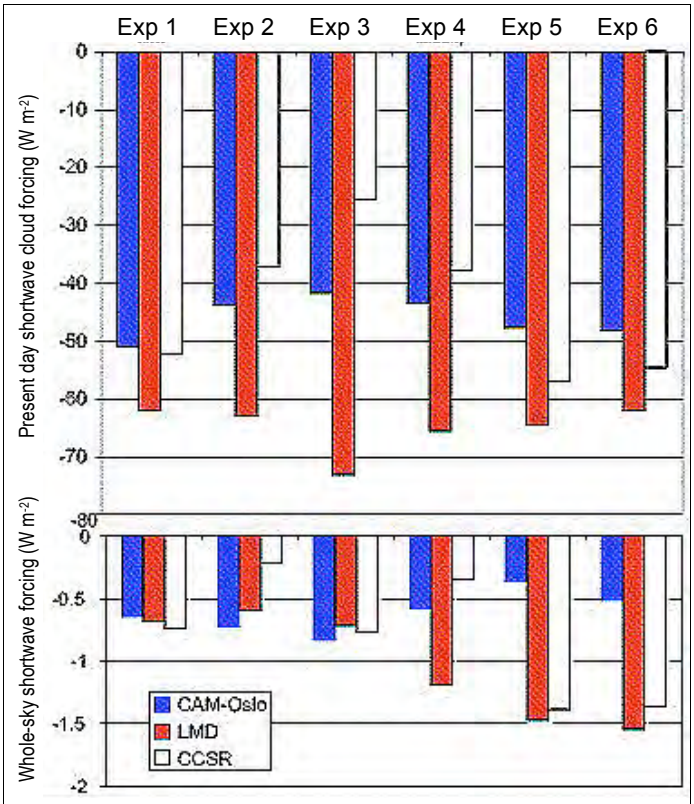

Fig. 3.6. Global average present day short wave cloud forcing at TOA (top) and change in whole sky net outgoing shortwave radiation (bottom) between the present-day and pre-industrial simulations for each model in each experiment. Adapted from Penner et al. (2006).

The change in cloud forcing is the difference between whole sky and clear sky outgoing radiation in the present day minus pre-industrial simulation. The large differences seen between experiments 5 and 6 are due to the inclusion of the clear sky component of aerosol scattering and absorption (the direct effect) in experiment 6.

In the second experiment, the aerosol mass and size distribution were again prescribed, but now each model used its own formulation for relating aerosols to droplets. In this case one of the models produced larger effective radii and therefore a much smaller first indirect aerosol effect (Figure 3.6, Table 3.5). However, even in the two models where the effective radius change and net global forcing were similar, the spatial patterns of cloud forcing differ, especially over the biomass burning regions of Africa and South America.

The third experiment allowed the models to relate the change in droplet size to change in precipitation efficiency (i.e., they were now also allowing the second indirect effect - smaller

droplets being less efficient rain producers – as well as the first). The models utilized the same relationship for autoconversion of cloud droplets to precipitation. Changing the precipitation efficiency results in all models producing an increase in cloud liquid water path, although the effect on cloud fraction was smaller than in the previous experiments. The net result was to increase the negative radiative forcing in all three models, albeit with different magnitudes: for two of the models the net impact on outgoing shortwave radiative increased by about 20%, whereas in the third model (which had the much smaller first indirect effect), it was magnified by a factor of three.

In the fourth experiment, the models were now each allowed to use their own formulation to relate aerosols to precipitation efficiency. This introduced some additional changes in the whole sky shortwave forcing (Figure 3.6).

In the fifth experiment, models were allowed to produce their own aerosol concentrations, but were given common sources. This produced the largest changes in the RF in several of the models. Within any one model, therefore, the change in aerosol concentration has the largest effect on droplet concentrations and effective radii. This experiment too resulted in large changes in RF.

Table 3.5. Differences (Wm^{-2}) in present day and pre-industrial outgoing solar radiation in the different experiments. Adapted from Penner et al. (2006).

MODEL	EXP 1	EXP 2	EXP 3	EXP 4	EXP 5	EXP 6
Whole-sky						
CAM-Oslo	-0.648	-0.726	-0.833	-0.580	-0.365	-0.518
LMD-Z	-0.682	-0.597	-0.722	-1.194	-1.479	-1.553
CCSR	-0.739	-0.218	-0.733	-0.350	-1.386	-1.386
Clear-sky						
CAM-Oslo	-0.063	-0.066	-0.026	0.014	-0.054	-0.575
LMD-Z	-0.054	0.019	0.030	-0.066	-0.126	-1.034
CCSR	0.018	-0.007	-0.045	-0.008	0.018	-1.160
Cloud-forcing						
CAM-Oslo	-0.548	-0.660	-0.807	-0.595	-0.311	0.056
LMD-Z	-0.628	-0.616	-0.752	-1.128	-1.353	-0.518
CCSR	-0.757	-0.212	-0.728	-0.345	-1.404	-0.200

EXP1: tests cloud formation and radiation schemes
EXP2: tests formulation for relating aerosols to droplets
EXP3: tests inclusion of droplet size influence on precipitation efficiency
EXP4: tests formulation of droplet size influece on precipitation efficiency
EXP5: tests model aerosol formulation from common sources
EXP6: added the direct aerosol effect

In the last experiment, the aerosol direct effect was included, based on the full range of aerosols used in each model. While the impact on the whole-sky forcing was not large, the addition of aerosol scattering and absorption primarily affected the change in clear sky radiation (Table 3.5).

The results of this study emphasize that in addition to questions concerning cloud physics, the differences in aerosol concentrations among the models play a strong role in inducing differences in the indirect effect(s), as well as the direct one.

Observational constraints on climate model simulations of the indirect effect with satellite data (e.g. MODIS) have been performed previously in a number of studies (e.g. Storelvmo et al. 2006, Lohmann et al. 2006, Quaas et al. 2006, Menon et al. 2008). These have been somewhat limited since the satellite retrieved data used do not have the vertical profiles needed to resolve aerosol and cloud fields (e.g. cloud droplet number and liquid water content); the temporal resolution of simultaneous aerosol and cloud product retrievals are usually not available at a frequency of more than one a day; and higher level clouds often obscure low clouds and aerosols. Thus, the indirect effect, especially the second indirect effect, remains, to a large extent,

unconstrained by satellite observations. However, improved measurements of aerosol vertical distribution from the newer generation of sensors on the A-train platform may provide a better understanding of changes to cloud properties from aerosols. Simulating the top-of-atmosphere reflectance for comparison to satellite measured values could be another way to compare model with observations, which would eliminate the inconsistent assumptions of aerosol optical properties and surface reflectance encountered when compared the model calculated and satellite retrieved AOD values.

3.4.3. Additional Aerosol Influences

Various observations have empirically related aerosols injected from biomass burning or industrial processes to reductions in rainfall (e.g., Warner, 1968; Eagan et al., 1974; Andreae et al., 2004; Rosenfeld, 2000). There are several potential mechanisms associated with this response.

In addition to the two indirect aerosol effects noted above, a process denoted as the "semi-direct" effect involves the absorption of solar radiation by aerosols such as black carbon and dust. The absorption increases the temperature, thus lowering the relative humidity and producing evaporation, hence a reduction in cloud liquid water. The impact of this process depends strongly on what the effective aerosol absorption actually is; the more absorbing the aerosol, the larger the potential positive forcing on climate (by reducing low level clouds and allowing more solar radiation to reach the surface). This effect is responsible for shifting the critical value of SSA (separating aerosol cooling from aerosol warming) from 0.86 with fixed clouds to 0.91 with varying clouds (Hansen et al., 1997). Reduction in cloud cover and liquid water is one way aerosols could reduce rainfall.

More generally, aerosols can alter the location of solar radiation absorption within the system, and this aspect alone can alter climate and precipitation even without producing any change in net radiation at the top of the atmosphere (the usual metric for climate impact). By decreasing solar absorption at the surface, aerosols (from both the direct and indirect effects) reduce the energy available for evapotranspiration, potentially resulting in a decrease in precipitation. This effect has been suggested as the reason for the decrease in pan evaporation over the last 50 years (Roderick and Farquhar, 2002). The decline in solar radiation at the surface appears to have ended in the 1990s (Wild et al., 2005), perhaps because of reduced aerosol emissions in industrial areas (Kruger and Grasl, 2002), although this issue is still not settled.

Energy absorption by aerosols above the boundary layer can also inhibit precipitation by warming the air at altitude relative to the surface, i.e., increasing atmospheric stability. The increased stability can then inhibit convection, affecting both rainfall and atmospheric circulation (Ramanathan et al., 2001a; Chung and Zhang, 2004). To the extent that aerosols decrease droplet size and reduce precipitation efficiency, this effect by itself could result in lowered rainfall values locally.

In their latest simulations, Hansen et al. (2007) did find that the indirect aerosol effect reduced tropical precipitation; however, the effect is similar regardless of which of the two indirect effects is used, and also similar to the direct effect. So it is likely that the reduction of tropical precipitation is because of aerosol induced cooling at the surface and the consequent reduced

evapotranspiration. Similar conclusions were reached by Yu et al. (2002) and Feingold et al. (2005). In this case, the effect is a feedback and not a forcing.

The local precipitation change, through its impacts on dynamics and soil moisture, can have large positive feedbacks. Harvey (2004) concluded from assessing the response to aerosols in 8 coupled models that the aerosol impact on precipitation was larger than on temperature. He also found that the precipitation impact differed substantially among the models, with little correlation among them.

Recent GCM simulations have further examined the aerosol effects on hydrological cycle. Ramanathan et al. (2005) showed from fully coupled ocean–atmosphere GCM experiments that the "solar dimming" effect at the surface, i.e., the reduction of solar radiation reaching the surface, due to the inclusion of absorbing aerosol forcing causes a reduction in surface evaporation, a decrease in meridional sea surface temperature (SST) gradient and an increase in atmospheric stability, and a reduction in rainfall over South Asia. Lau and Kim (2006) examined the direct effects of aerosol on the monsoon water cycle variability from GCM simulations with prescribed realistic global aerosol forcing and proposed the "elevated heat pump" effect, suggesting that atmospheric heating by absorbing aerosols (dust and black carbon), through water cycle feedback, may lead to a strengthening of the South Asia monsoon. These model results are not necessarily at odds with each other, but rather illustrate the complexity of the aerosol–monsoon interactions that are associated with different mechanisms, whose relative importance in affecting the monsoon may be strongly dependent on spatial and temporal scales and the timing of the monsoon. These results may be model dependent and should be further examined.

3.4.4. High Resolution Modeling

Largely by its nature, the representation of the interaction between aerosol and clouds in GCMs is poorly resolved. This stems in large part from the fact that GCMs do not resolve convection on their large grids (order of several hundred km), that their treatment of cloud microphysics is rather crude, and that as discussed previously, their representation of aerosol needs improvement. Superparametrization efforts (where standard cloud parameterizations in the GCM are replaced by resolving clouds in each grid column of the GCM via a cloud resolving model, e.g., Grabowski, 2004) could lead the way for the development of more realistic cloud fields and thus improved treatments of aerosol-cloud interactions in large-scale models. However, these are just being incorporated in models that resolve both cloud and aerosols. Detailed cloud parcel models have been developed to focus on the droplet activation problem (that asks under what conditions droplets actually start forming) and questions associated with the first indirect effect. The coupling of aerosol and cloud modules to dynamical models that resolve the large turbulent eddies associated with vertical motion and clouds [large eddy simulations (LES) models, with grid sizes of ~ 100 m and domains ~ 10 km] has proven to be a powerful tool for representing the details of aerosol-cloud interactions together with feedbacks (e.g., Feingold et al. 1994; Kogan et al. 1994; Stevens et al, 1996; Feingold et al. 1999; Ackerman et al. 2004). This section explores some of the complexity in the aerosol indirect effects revealed by such studies to illustrate how difficult parameterizing these effects properly in GCMs could really be.

3.4.4a. The first indirect effect

The relationship between aerosol and drop concentrations (or drop sizes) is a key piece of the first indirect effect puzzle. (It should not, however, be equated to the first indirect effect which concerns itself with the resultant RF). A huge body of measurement and modeling work points to the fact that drop concentrations increase with increasing aerosol. The main unresolved questions relate to the degree of this effect, and the relative importance of aerosol size distribution, composition and updraft velocity in determining drop concentrations (for a review, see McFiggans et al., 2006). Studies indicate that the aerosol number concentration and size distribution are the most important aerosol factors. Updraft velocity (unresolved by GCMs) is particularly important under conditions of high aerosol particle number concentration.

Although it is likely that composition has some effect on drop number concentrations, composition is generally regarded as relatively unimportant compared to the other parameters (Fitzgerald, 1975; Feingold, 2003; Ervens et al., 2005; Dusek et al., 2006). Therefore, it has been stated that the significant complexity in aerosol composition can be modeled, for the most part, using fairly simple parameterizations that reflect the soluble and insoluble fractions (e.g., Rissler et al. 2004). However, composition cannot be simply dismissed. Furthermore, chemical interactions also cannot be overlooked. A large uncertainty remains concerning the impact of organic species on cloud droplet growth kinetics, thus cloud droplet formation. Cloud drop size is affected by wet scavenging, which depends on aerosol composition especially for freshly emitted aerosol. And future changes in composition will presumably arise due to biofuels/biomass burning and a reduction in sulfate emissions, which emphasizes the need to include composition changes in models when assessing the first indirect effect. The simple soluble/insoluble fraction model may become less applicable than is currently the case.

The updraft velocity, and its change as climate warms, may be the most difficult aspect to simulate in GCMs because of the small scales involved. In GCMs it is calculated in the dynamics as a grid box average, and parameterized on the small scale indirectly because it is a key part of convection and the spatial distribution of condensate, as well as droplet activation. Numerous solutions to this problem have been sought, including estimation of vertical velocity based on predicted turbulent kinetic energy from boundary layer models (Lohmann et al., 1999; Larson et al., 2001) and PDF representations of subgrid quantities, such as vertical velocity and the vertically-integrated cloud liquid water ('liquid water path', or LWP) (Pincus and Klein, 2000; Golaz et al., 2002a,b; Larson et al., 2005). Embedding cloud-resolving models within GCMs is also being actively pursued (Grabowski et al. 1999; Randall et al., 2003). Numerous other details come into play; for example, the treatment of cloud droplet activation in GCM frameworks is often based on the assumption of adiabatic conditions, which may overestimate the sensitivity of cloud to changes in CCN (Sotiropoulou et al., 2006, 2007). This points to the need for improved theoretical understanding followed by new parameterizations.

3.4.4b. Other indirect effects

The second indirect effect is often referred to as the "cloud lifetime effect", based on the premise that non-precipitating clouds will live longer. In GCMs the "lifetime effect" is equivalent to changing the representation of precipitation production and can be parameterized as an increase in cloud area or cloud cover (e.g., Hansen et al., 2005). The second indirect effect hypothesis states that the more numerous and smaller drops associated with aerosol perturbations, suppress collision-induced rain, and result in a longer cloud lifetime. Observational evidence for the

suppression of rain in warm clouds exists in the form of isolated studies (e.g. Warner, 1968) but to date there is no statistically robust proof of surface rain suppression (Levin and Cotton, 2008). Results from ship-track studies show that cloud water may increase or decrease in the tracks (Coakley and Walsh, 2002) and satellite studies suggest similar results for warm boundary layer clouds (Han et al. 2002). Ackerman et al. (2004) used LES to show that in stratocumulus, cloud water may increase or decrease in response to increasing aerosol depending on the relative humidity of the air overlaying the cloud. Wang et al. (2003) showed that all else being equal, polluted stratocumulus clouds tend to have lower water contents than clean clouds because the small droplets associated with polluted clouds evaporate more readily and induce an evaporation-entrainment feedback that dilutes the cloud. This result was confirmed by Xue and Feingold (2006) and Jiang and Feingold (2006) for shallow cumulus, where pollution particles were shown to decrease cloud fraction. Furthermore, Xue et al. (2008) suggested that there may exist two regimes: the first, a precipitating regime at low aerosol concentrations where an increase in aerosol will suppress precipitation and increase cloud cover (Albrecht, 1989); and a second, non precipitating regime where the enhanced evaporation associated with smaller drops will decrease cloud water and cloud fraction.

The possibility of bistable aerosol states was proposed earlier by Baker and Charlson (1990) based on consideration of aerosol sources and sinks. They used a simple numerical model to suggest that the marine boundary layer prefers two aerosol states: a clean, oceanic regime characterized by a weak aerosol source and less reflective clouds; and a polluted, continental regime characterized by more reflective clouds. On the other hand, study by Ackerman et al. (1994) did not support such a bistable system using a somewhat more sophisticated model. Further observations are needed to clarify the nature of cloud/aerosol interactions under a variety of conditions.

Finally, the question of possible effects of aerosol on cloud lifetime was examined by Jiang et al. (2006), who tracked hundreds of cumulus clouds generated by LES from their formative stages until they dissipated. They showed that in the model there was no effect of aerosol on cloud lifetime, and that cloud lifetime was dominated by dynamical variability.

It could be argued that the representation of these complex feedbacks in GCMs is not warranted until a better understanding of the processes is at hand. Moreover, until GCMs are able to represent cloud scales, it is questionable what can be obtained by adding microphysical complexity to poorly resolved clouds. A better representation of aerosol-cloud interactions in GCMs therefore depends on ability to improve representation of aerosols and clouds, and indeed the entire hydrologic cycle, as well as their interaction. This issue is discussed further in the next chapter.

3.5. Aerosol in the Climate Models

3.5.1. Aerosol in the IPCC AR4 Climate Model Simulations

To assess the atmospheric and climate response to aerosol forcing, e.g., changes in surface temperate, precipitation, or atmospheric circulation, aerosols, together with greenhouse gases should be an integrated part of climate model simulation under the past, present, and future conditions. **Table 3.6** lists the forcing species that were included in 25 climate modeling groups used in the IPCC AR4 (2007) assessment. All the models included long-lived greenhouse gases,

most models included sulfate direct forcing, but only a fraction of those climate models considered other aerosol types. In other words, aerosol RF was not adequately accounted for in the climate simulations for the IPCC AR4. Put still differently, the current aerosol modeling capability has not been fully incorporated into the climate model simulations. As pointed out in Section 3.4, fewer than one-third of the models incorporated an aerosol indirect effect, and most considered only sulfates.

Table 3.6. Forcings used in IPCC AR4 simulations of 20th century climate change. This Table is adapted from SAP 1.1 Table 5.2 (compiled using information provided by the participating modeling centers, see http://www-pcmdi.llnl.gov/ipcc/model_documentation/ipcc_model_documentation.php) plus additional information from that website. Eleven different forcings are listed: well-mixed greenhouse gases (G), tropospheric and stratospheric ozone (O), sulfate aerosol direct (SD) and indirect effects (S), black carbon (BC) and organic carbon aerosols (OC), mineral dust (MD), sea salt (SS), land use/land cover (LU), solar irradiance (SO), and volcanic aerosols (V). Check mark denotes inclusion of a specific forcing. As used here, "inclusion" means specification of a time-varying forcing, with changes on interannual and longer timescales.

	MODEL	COUNTRY	G	O	SD	SI	BC	OC	MD	SS	LU	SO	V
1	BCC-CM1	China	√	√	√								
2	BCCR-BCM2.0	Norway	√		√				√	√			
3	CCSM3	USA	√	√	√		√	√				√	√
4	CGCM3.1(T47)	Canada	√		√								
5	CGCM3.1(T63)	Canada	√		√								
6	CNRM-CM3	France	√	√	√		√						
7	CSIRO-Mk3.0	Australia	√		√								
8	CSIRO-Mk3.5	Australia	√		√								
9	ECHAM5/MPI-OM	Germany	√	√	√	√							
10	ECHO-G	Germany/Korea	√	√	√	√						√	√
11	FGOALS-g1.0	China	√		√								
12	GFDL-CM2.0	USA	√	√	√		√	√			√	√	√
13	GFDL-CM2.1	USA	√	√	√		√	√			√	√	√
14	GISS-AOM	USA	√		√					√			
15	GISS-EH	USA	√	√	√	√	√	√	√	√	√	√	√
16	GISS-ER	USA	√	√	√	√	√	√	√	√	√	√	√
17	INGV-SXG	Italy	√	√	√								
18	INM-CM3.0	Russia	√		√							√	
19	IPSL-CM4	France	√		√	√							
20	MIROC3.2(hires)	Japan	√	√	√		√	√	√	√	√	√	√
21	MIROC3.2(medres)	Japan	√	√	√		√	√	√	√	√	√	√
22	MRI-CGCM2.3.2	Japan	√		√							√	√
23	PCM	USA	√	√	√							√	√
24	UKMO-HadCM3	UK	√	√	√	√							
25	UKMO-HadGEM1	UK	√	√	√	√	√	√			√	√	√

The following discussion compares two of the IPCC AR4 climate models that include all major forcing agencies in their climate simulation: The model from the NASA Goddard Institute for Space Studies (GISS) and from the NOAA Geophysical Fluid Dynamics Laboratory (GFDL).

The purpose in presenting these comparisons is to help elucidate how modelers go about assessing their aerosol components, and the difficulties that entail. A particular concern is how aerosol forcings were obtained in the climate model experiments for IPCC AR4. Comparisons with observations have already led to some improvements that can be implemented in climate models for subsequent climate change experiments (e.g., Koch et al., 2006, for GISS model). This aspect is discussed further in chapter 4.

3.5.1a. The GISS model

There have been many different configurations of aerosol simulations in the GISS model over the years, with different emissions, physics packages, etc., as is apparent from the multiple GISS entries in the preceding figures and tables. There were also three different GISS GCM submissions to IPCC AR4, which varied in their model physics and ocean formulation. (Note that the aerosols in these three GISS versions are different from those in the AeroCom simulations described in section 3.2 and 3.3.) The GCM results discussed below all relate to the simulations known as GISS model ER (Schmidt et al., 2006, see Table 3.6).

Although the detailed description and model evaluation have been presented in Liu et al. (2006), below are the general characteristics of aerosols in the GISS ER:

Aerosol fields: The aerosol fields used in the GISS ER is a prescribed "climatology" which is obtained from chemistry transport model simulations with monthly averaged mass concentrations representing conditions up to1990. Aerosol species included are sulfate, nitrate, BC, POM, dust, and sea salt. Dry size effective radii are specified for each of the aerosol types, and laboratory-measured phase functions are employed for all solar and thermal wavelengths. For hygroscopic aerosols (sulfate, nitrate, POM, and sea salt), formulas are used for the particle growth of each aerosol as a function of relative humidity, including the change in density and optical parameters. With these specifications, the AOD, single scattering albedo, and phase function of the various aerosols are calculated. While the aerosol distribution is prescribed as monthly mean values, the relative humidity component of the extinction is updated each hour. The global averaged AOD at 550 nm is about 0.15.

Global distribution: When comparing with AOD from observations by multiple satellite sensors of MODIS, MISR, POLDER, and AVHRR and surface based sunphotometer network AERONET (see chapter 2 for detailed information about data), qualitative agreement is apparent, with generally higher burdens in Northern Hemisphere summer, and seasonal variations of smoke over southern Africa and South America, as well as wind blown dust over northern African and the Persian Gulf. Aerosol optical depth in both model and observations is smaller away from land. There are, however, considerable discrepancies between the model and observations. Overall, the GISS GCM has reduced aerosol optical depths compared with the satellite data (a global, clear-sky average of about 80% compared with MODIS and MISR data), although it is in better agreement with AERONET ground-based measurements in some locations (note that the input aerosol values were calibrated with AERONET data). The model values over the Sahel in Northern Hemisphere winter and the Amazon in Southern Hemisphere winter are excessive, indicative of errors in the biomass burning distributions, at least partially associated with an older biomass burning source used (the source used here was from Liousse et al., 1996).

Seasonal variation: A comparison of the seasonal distribution of the global AOD between the GISS model and satellite data indicates that the model seasonal variation is in qualitative agreement with observations for many of the locations that represent major aerosol regimes, although there are noticeable differences. For example, in some locations the seasonal variations are different from or even opposite to the observations.

Particle size parameter: The Ångström exponent (Å), which is determined by the contrast between the AOD at two or more different wavelengths and is related to aerosol particle size (discussed in section 3.3). This parameter is important because the particle size distribution affects the efficiency of scattering of both short and long wave radiation, as discussed earlier. Å from the GISS model is biased low compared with AERONET, MODIS, and POLDER data, although there are technical differences in determining the Å. This low bias suggests that the aerosol particle size in the GISS model is probably too large. The average effective radius in the GISS model appears to be 0.3-0.4 μm, whereas the observational data indicates a value more in the range of 0.2-0.3 μm (Liu et al., 2006).

Single scattering albedo: The model-calculated SSA (at 550 nm) appears to be generally higher than the AERONET data at worldwide locations (not enough absorption), but lower than AERONET data in Northern Africa, the Persian Gulf, and the Amazon (too much absorption). This discrepancy reflects the difficulties in modeling BC, which is the dominant absorbing aerosol, and aerosol sizes. Global averaged SSA at 550 nm from the GISS model is at about 0.95.

Aerosol direct RF: The GISS model calculated aerosol direct shortwave RF is -0.56 W m^{-2} at TOA and -2.87 W m^{-2} at the surface. The TOA forcing (upper left, **Figure 3.7**) indicates that, as expected, the model has larger negative values in polluted regions and positive forcing at the highest latitudes. At the surface (lower left, Figure 3.7) GISS model values exceed -4 W m^{-2} over large regions. Note that these results are for the model's total aerosols (anthropogenic plus natural) and thus differ from the anthropogenic aerosol effect discussed earlier (section 3.3 and Figure 3.3). Note there is also a longwave RF of aerosols (right column), although they are much weaker than the shortwave RF.

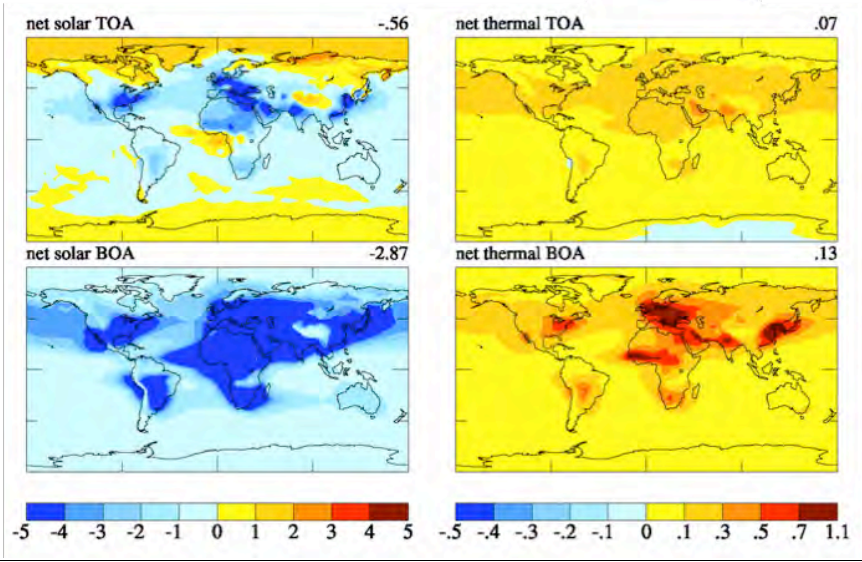

Fig. 3.7. Direct radiative forcing by anthropogenic aerosols in the GISS model (including sulfates, BC, OC and nitrates). Short wave forcing at TOA and surface are shown in the top left and bottom left panels. The corresponding thermal forcing is indicated in the right hand panels. Figure provided by A. Lacis, GISS.

There are several concerns for climate change simulations related to the aerosol trend in the GISS model. One is that the aerosol fields in the GISS AR4 climate simulation (version ER) are kept fixed after 1990. In fact, the observed trend shows a reduction in tropospheric aerosol optical thickness from 1990 through the present, at least over the oceans (Mishchenko and Geogdzhayev, 2007). Hansen et al. (2007) suggested that the deficient warming in the GISS model over Eurasia post-1990 was due to the lack of this trend. Indeed, a possible conclusion from the Penner et al. (2002) study was that the GISS model overestimated the AOD (presumably associated with anthropogenic aerosols) poleward of 30°N. However, when an alternate experiment reduced the aerosol optical depths, the polar warming became excessive (Hansen et al., 2007). The other concern is that the GISS model may underestimate the organic and sea salt AOD, and overestimate the influence of black carbon aerosols in the biomass burning regions (deduced from Penner et al., 2002; Liu et al., 2006). To the extent that is true, it would indicate the GISS model underestimates the aerosol direct cooling effect in a substantial portion of the tropics, outside of biomass burning areas. Clarifying those issues requires numerous modeling experiments and various types of observations.

3.5.1b. The GFDL model

A comprehensive description and evaluation of the GFDL aerosol simulation are given in Ginoux et al. (2006). Below are the general characteristics:

Aerosol fields: The aerosols used in the GFDL climate experiments are obtained from simulations performed with the MOZART 2 model (Model for Ozone and Related chemical Tracers) (Horowitz et al., 2003; Horozwitz, 2006). The exceptions were dust, which was generated with a separate simulation of MOZART 2, using sources from Ginoux et al. (2001) and wind fields from NCEP/NCAR reanalysis data; and sea salt, whose monthly mean concentrations were obtained from a previous study by Haywood et al. (1999). It includes most of the same aerosol species as in the GISS model (although it does not include nitrates), and, as in the GISS model, relates the dry aerosol to wet aerosol optical depth via the model's relative humidity for sulfate (but not for organic carbon); for sea salt, a constant relative humidity of 80% was used. Although the parameterizations come from different sources, both models maintain a very large growth in sulfate particle size when the relative humidity exceeds 90%.

Global distributions: Overall, the GFDL global mean aerosol mass loading is within 30% of that of other studies (Chin et al., 2002; Tie et al., 2005; Reddy et al., 2005a), except for sea salt, which is 2 to 5 times smaller. However, the sulfate AOD (0.1) is 2.5 times that of other studies, whereas the organic carbon value is considerably smaller (on the order of 1/2). Both of these differences are influenced by the relationship with relative humidity. In the GFDL model, sulfate is allowed to grow up to 100% relative humidity, but organic carbon does not increase in size as relative humidity increases. Comparison of AOD with AVHRR and MODIS data for the time period 1996-2000 shows that the global mean value over the ocean (0.15) agrees with AVHRR data (0.14) but there are significant differences regionally, with the model overestimating the value in the northern mid latitude oceans and underestimating it in the southern ocean. Comparison with MODIS also shows good agreement globally (0.15), but in this case indicates large disagreements over land, with the model producing excessive AOD over industrialized countries and underestimating the effect over biomass burning regions. Overall, the global averaged AOD at 550 nm is 0.17, which is higher than the maximum values in the AeroCom-A experiments (Table 3.2) and exceeds the observed value too (Ae and S* in Figure 3.1).

Composition: Comparison of GFDL modeled species with *in situ* data over North America, Europe, and over oceans has revealed that the sulfate is overestimated in spring and summer and underestimated in winter in many regions, including Europe and North America. Organic and black carbon aerosols are also overestimated in polluted regions by a factor of two, whereas organic carbon aerosols are elsewhere underestimated by factors of 2 to 3. Dust concentrations at the surface agree with observations to within a factor of 2 in most places where significant dust exists, although over the southwest U.S. it is a factor of 10 too large. Surface concentrations of sea salt are underestimated by more than a factor of 2. Over the oceans, the excessive sulfate AOD compensates for the low sea salt values except in the southern oceans.

Size and single-scattering albedo: No specific comparison was given for particle size or single-scattering albedo, but the excessive sulfate would likely produce too high a value of reflectivity relative to absorption except in some polluted regions where black carbon (an absorbing aerosol) is also overestimated.

As in the case of the GISS model, there are several concerns with the GFDL model. The good global-average agreement masks an excessive aerosol loading over the Northern Hemisphere (in particular, over the northeast U.S. and Europe) and an underestimate over biomass burning regions and the southern oceans. Several model improvements are needed, including better parameterization of hygroscopic growth at high relative humidity for sulfate and organic carbon; better sea salt simulations; correcting an error in extinction coefficients; and improved biomass burning emissions inventory (Ginoux et al., 2006).

3.5.1c. Comparisons between GISS and GFDL model

Both GISS and GFDL models were used in the IPCC AR4 climate simulations for climate sensitivity that included aerosol forcing. It would be constructive, therefore, to compare the similarities and differences of aerosols in these two models and to understand what their impacts are in climate change simulations. **Figure 3.8** shows the percentage AOD from different aerosol components in the two models.

Sulfate: The sulfate AOD from the GISS model is within the range of that from all other models (Table 3.3), but that from the GFDL model exceeds the maximum value by a factor of 2.5. An assessment in SAP 3.2 (2008; Shindell et al., 2008b) also concludes that GFDL had excessive sulfate AOD compared with other models. The sulfate AOD from GFDL is nearly a factor of 4 large than that from GISS, although the sulfate burden differs only by about 50% between the two models. Clearly, this implies a large difference in sulfate MEE between the two models.

BC and POM: Compared to observations, the GISS model appears to overestimate the influence of BC and POM in the biomass burning regions and underestimate it elsewhere, whereas the GFDL model is somewhat the reverse: it overestimates it in polluted regions, and underestimates it in biomass burning areas. The global comparison shown in Table 3.4 indicates the GISS model has values similar to those from other models, which might be the result of such compensating errors. The GISS and GFDL models have relatively similar global-average black carbon contributions, and the same appears true for POM.

Sea salt: The GISS model has a much larger sea salt contribution than does GFDL (or indeed other models).

Global and regional distributions: Overall, the global averaged AOD is 0.15 from the GISS model and 0.17 from GFDL. However, as shown in Figure 3.8, the contribution to this AOD from different aerosol components shows greater disparity. For example, over the Southern Ocean where the primary influence is due to sea salt in the GISS model, but in the GFDL it is sulfate. The lack of satellite observations of the component contributions and the limited available *in situ* measurements make the model improvements at aerosol composition level difficult.

Climate simulations: With such large differences in aerosol composition and distribution between the GISS and GFDL models, one might expect that the model simulated surface temperature might be quite different. Indeed, the GFDL model was able to reproduce the observed temperature change during the 20th century without the use of an indirect aerosol effect, whereas the GISS model required a substantial indirect aerosol contribution (more than half of the total aerosol forcing; Hansen et al., 2007). It is likely that the reason for this difference was the excessive direct effect in the GFDL model caused by its overestimation of the sulfate optical depth. The GISS model direct aerosol effect (see Section 3.6) is close to that derived from observations (Chapter 2); this suggests that for models with climate sensitivity close to 0.75°C/(W m^{-2}) (as in the GISS and GFDL models), an indirect effect is needed.

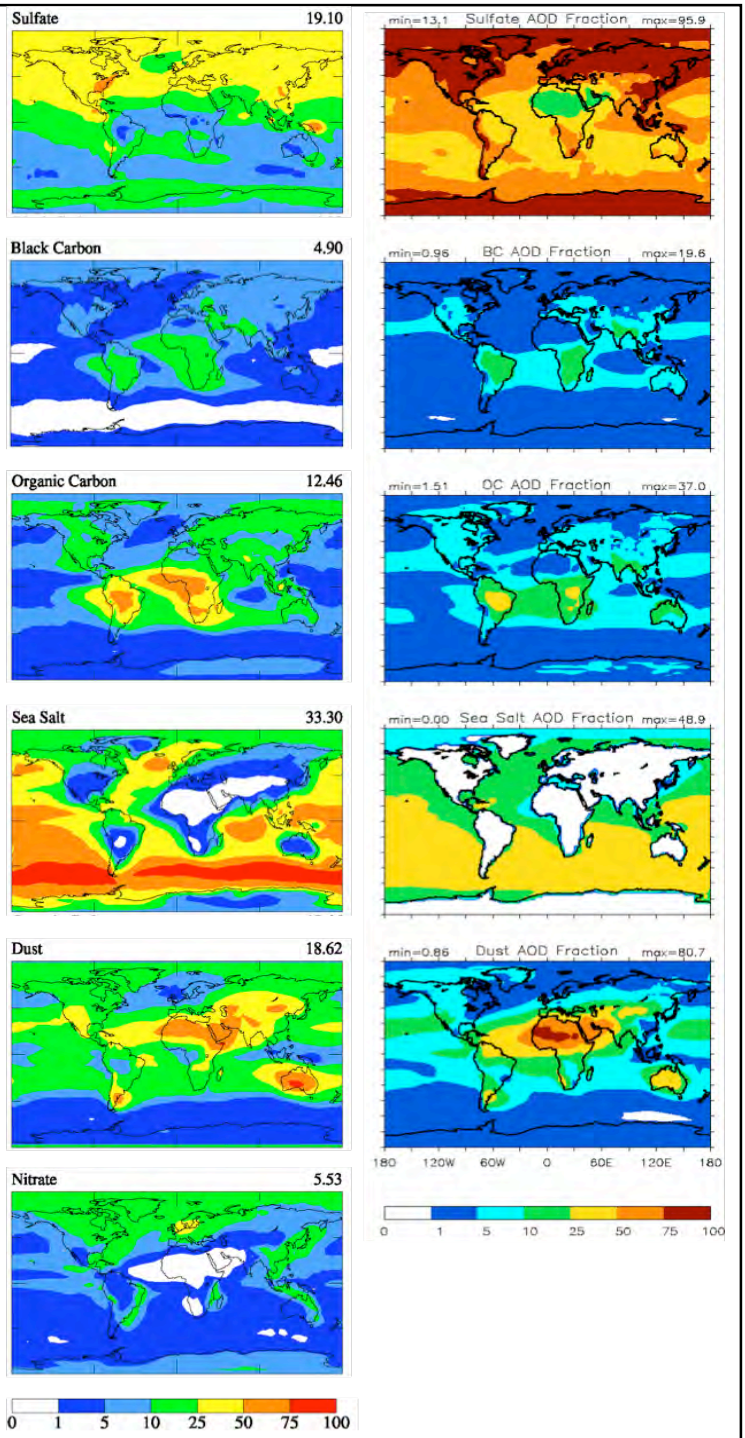

Fig. 3.8. Percentage of aerosol optical depth in the GISS (left, based on Liu et al., 2006, provided by A. Lacis, GISS) and GFDL (right, from Ginoux et al., 2006) models associated with the different components: Sulfate (1st row), BC (2nd row), OC (3rd row), sea-salt (4th row), dust (5th row), and nitrate (last row. Nitrate not available in GFDL model). Numbers on the GISS panels are global average but on the GFDL panels are maximum and minimum.

3.5.2. Additional considerations

Long wave aerosol forcing: So far only the aerosol RF in the shortwave (solar) spectrum has been discussed. Figure 3.7 (right column) shows that compared to the shortwave forcing, the values of aerosol long wave (thermal) forcing in the GISS model are on the order of 10%, with contribution coming mainly from dust aerosol. Like the shortwave forcing, these values will also be affected by the particular aerosol characteristics used in the simulation.

Aerosol vertical distribution: Vertical distribution is particularly important for absorbing aerosols, such as BC and dust in calculating the RF, particularly when longwave forcing is considered (e.g. Figure 3.7) because the energy they reradiate depends on the temperature (and hence altitude), which affects the calculated forcing values. Several model inter-comparison studies have shown that the largest difference among model simulated aerosol distributions is the vertical profile (e.g. Lohmann et al., 2001; Penner et al., 2002; Textor et al., 2006), due to the significant diversities in atmospheric processes in the models (e.g., Table 3.2). In addition, the vertical distribution also varies with space and time, as illustrated in **Figure 3.9** from the GISS ER simulations for January and July showing the most probable altitude of aerosol vertical locations. In general, aerosols in the northern hemisphere are located at lower altitudes in January than in July, and vice versa for the southern hemisphere.

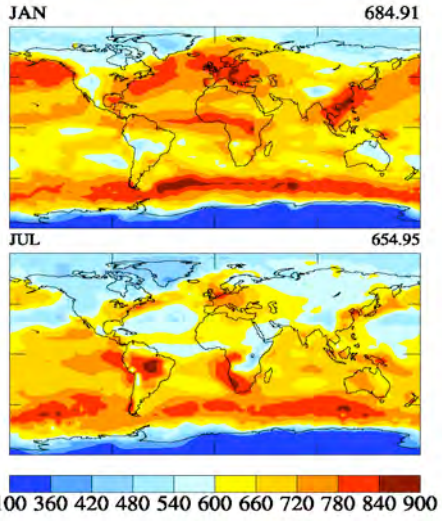

Fig. 3.9. Most probable aerosol altitude (in pressure, hPa) from the GISS model in January (top) and July (bottom). Figure from A. Lacis, GISS.

Mixing state: Most climate model simulations incorporating different aerosol types have been made using external mixtures, i.e., the evaluation of the aerosols and their radiative properties are calculated separately for each aerosol type (assuming no mixing between different components within individual particles). Observations indicate that aerosols commonly consist of internally mixed particles, and these "internal mixtures" can have very different radiative impacts. For example, the GISS-1 (internal mixture) and GISS-2 (external mixture) model results shows very different magnitude and sign of aerosol forcing from slightly positive (implying slight warming) to strong negative (implying significant cooling) TOA forcing (Figure 3.2), due to changes in both radiative properties of the mixtures, and in aerosol amount. The more sophisticated aerosol mixtures from detailed microphysics calculations now being used/developed by different modeling groups may well end up producing very different direct (and indirect) forcing values.

Cloudy sky vs. clear sky: The satellite or AERONET observations are all for clear sky only because aerosol cannot be measured in the remote sensing technique when clouds are present. However, almost all the model results are for all-sky because of difficulty in extracting cloud-free scenes from the GCMs. So the AOD comparisons discussed earlier are not completely consistent. Because AOD can be significantly amplified when relative humidity is high, such as near or inside clouds, all-sky AOD values are expected to be higher than clear sky AOD values. On the other hand, the aerosol RF at TOA is significantly lower for all-sky than for clear sky conditions; the IPCC AR4 and AeroCom RF study (Schulz et al., 2006) have shown that on

average the aerosol RF value for all-sky is about 1/3 of that for clear sky although with large diversity (63%). These aspects illustrate the complexity of the system and the difficulty of representing aerosol radiative influences in climate models whose cloud and aerosol distributions are somewhat problematic. And of course aerosols in cloudy regions can affect the clouds themselves, as discussed in Section 3.4.

3.6. Impacts of Aerosols on Climate Model Simulations

3.6.1. Surface Temperature Change

It was noted in the introduction that aerosol cooling is essential in order for models to produce the observed global temperature rise over the last century, at least models with climate sensitivities in the range of 3°C for doubled CO_2 (or ~0.75°C/Wm^{-2}). The implications of this are discussed here in somewhat more detail.

Hansen et al. (2007) show that in the GISS model, well-mixed greenhouse gases produce a warming of close to 1°C between 1880 and the present (**Table 3.7**). The direct effect of tropospheric aerosols as calculated in that model produces cooling of close to -0.3°C between those same years, while the indirect effect (represented in that study as cloud cover change) produces an additional cooling of similar magnitude (note that the general model result quoted in IPCC AR4 is that the indirect RF is twice that of the direct effect).

The time dependence of the total aerosol forcing used as well as the individual species components is shown in **Figure 3.10**. The resultant warming, 0.53 (±0.04) °C including these and other forcings (Table 3.7), is less than the observed value of 0.6-0.7°C from 1880-2003. Hansen et al. (2007) further show that a reduction in sulfate optical thickness and the direct aerosol effect by 50%, which also reduced the aerosol indirect effect by 18%, produces a negative aerosol forcing from 1880 to 2003 of –0.91 W m^{-2} (down from –1.37 W m^{-2} with this revised forcing). The model now warms 0.75°C over that time. Hansen et al. (2007) defend this change by noting that sulfate aerosol removal over North America and western Europe during the 1990s led to a cleaner atmosphere. Note that the comparisons shown in the previous section suggest that the GISS model already underestimates aerosol optical depths; it is thus trends that are the issue here.

Table 3.7. Climate forcings (1880-2003) used to drive GISS climate simulations, along with the surface air temperature changes obtained for several periods. Instantaneous (Fi), adjusted (Fa), fixed SST (Fs) and effective (Fe) forcings are defined in Hansen et al. 2005. From Hansen et al., 2007.

Forcing agent	Forcing W m^{-2} (1880 – 2003)				ΔT surface °C (year to 2003)			
	Fi	Fa	Fs	Fe	1880	1900	1950	1979
Well-mixed GHGs	2.62	2.50	2.65	2.72	0.96	0.93	0.74	0.43
Stratospheric H_2O	-	-	0.06	0.05	0.03	0.01	0.05	0.00
Ozone	0.44	0.28	0.26	0.23	0.08	0.05	0.00	-0.01
Land Use	-	-	-0.09	-0.09	-0.05	-0.07	-0.04	-0.02
Snow albedo	0.05	0.05	0.14	0.14	0.03	0.00	0.02	-0.01
Solar Irradiance	0.23	0.24	0.23	0.22	0.07	0.07	0.01	0.02
Stratospheric aerosols	0.00	0.00	0.00	0.00	-0.08	-0.03	-0.06	0.04
Trop. aerosol direct forcing	-0.41	-0.38	-0.52	-0.60	-0.28	-0.23	-0.18	-0.10
Trop. aerosol indirect forcing	-	-	-0.87	-0.77	-0.27	-0.29	-0.14	-0.05
Sum of above	**-**	**-**	**1.86**	**1.90**	**0.49**	**0.44**	**0.40**	**0.30**
All forcings at once	**-**	**-**	**1.77**	**1.75**	**0.53**	**0.61**	**0.44**	**0.29**

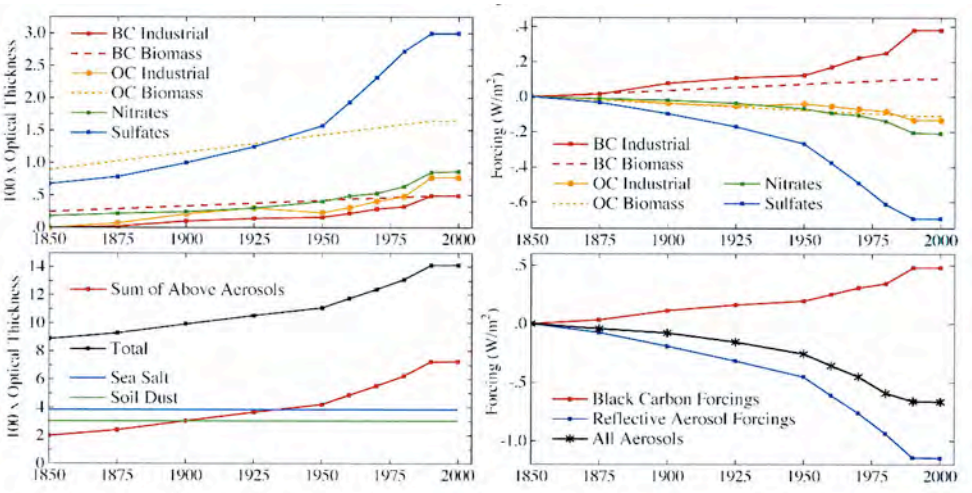

Fig. 3.10. Time dependence of aerosol optical thickness (left) and effect climate forcing (right). Note that as specified, the aerosol trends are all 'flat' from 1990 to 2000. From Hansen et al. (2007).

The magnitude of the indirect effect used by Hansen et al. (2005) is roughly calibrated to reproduce the observed change in diurnal temperature cycle and is consistent with some satellite observations. However, as Anderson et al., (2003) note, the forward calculation of aerosol negative forcing covers a much larger range than is normally used in GCMs; the values chosen, as in this case, are consistent with the inverse reasoning estimates of what is needed to produce the observed warming, and hence generally consistent with current model climate sensitivities. The authors justify this approach by claiming that paleoclimate data indicate a climate sensitivity of close to 0.75°(±0.25) °C/Wm^{-2}, and therefore something close to this magnitude of negative forcing is reasonable. Even this stated range leaves significant uncertainty in climate sensitivity and the magnitude of the aerosol negative forcing. Furthermore, IPCC (2007) concluded that paleoclimate data are not capable of narrowing the range of climate sensitivity, nominally 0.375 to 1.13 °C/Wm^{-2}, because of uncertainties in paleoclimate forcing and response; so from this perspective the total aerosol forcing is even less constrained than the GISS estimate. Hansen et al. (2007) acknowledge that "an equally good match to observations probably could be obtained from a model with larger sensitivity and smaller net forcing, or a model with smaller sensitivity and larger forcing".

The GFDL model results for global mean ocean temperature change (down to 3 km depth) for the time period 1860 to 2000 is shown in **Figure 3.11**, along with the different contributing factors (Delworth et al., 2005). This is the same GFDL model whose aerosol distribution was discussed previously. The aerosol forcing produces a cooling on the order of 50% that of greenhouse warming (generally similar to that calculated by the GISS model, Table 3.7). Note that this was achieved without any aerosol indirect effect.

The general model response noted by IPCC, as discussed in the introduction, was that the total aerosol forcing of -1.3 W m^{-2} reduced the greenhouse forcing of near 3 W m^{-2} by about 45%, in the neighborhood of the GFDL and GISS forcings. Since the average model sensitivity was close to 0.75 °C/Wm^{-2}, similar to the sensitivities of these models, the necessary negative forcing is

therefore similar. The agreement cannot therefore be used to validate the actual aerosol effect until climate sensitivity itself is better known.

Is there some way to distinguish between greenhouse gas and aerosol forcing that would allow the observational record to indicate how much of each was really occurring? This question of attribution has been the subject of numerous papers, and the full scope of the discussion is beyond the range of this report. It might be briefly noted that Zhang et al. (2006) using results from several climate models and including both spatial and temporal patterns, found that the climate responses to greenhouse gases and sulfate aerosols are correlated, and separation is possible only occasionally, especially at global scales. This conclusion appears to be both model and method-dependent: using time-space distinctions as opposed to trend detection may work differently in different models (Gillett et al., 2002a). Using multiple models helps primarily by providing larger-ensemble sizes for statistics (Gillett et al., 2002b). However, even separating between the effects of different aerosol types is difficult. Jones et al. (2005) concluded that currently the pattern of temperature change due to black carbon is indistinguishable from the sulfate aerosol pattern. In contrast, Hansen et al. (2005) found that absorbing aerosols produce a different global response than other forcings, and so may be distinguishable. Overall, the similarity in response to all these very different forcings is undoubtedly due to the importance of climate feedbacks in amplifying the forcing, whatever its nature.

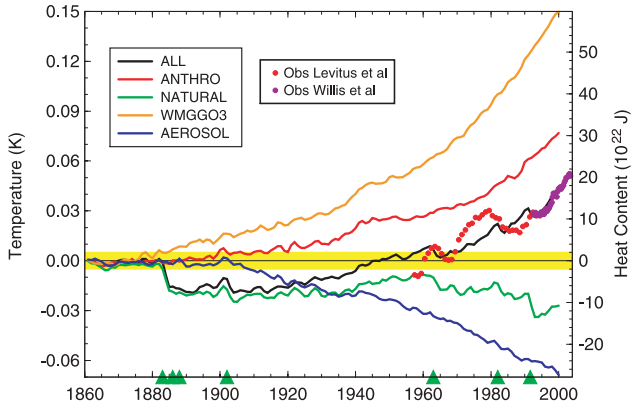

Fig. 3.11. Change in global mean ocean temperature (left axis) and ocean heat content (right axis) for the top 3000 m due to different forcings in the GFDL model. WMGG includes all greenhouse gases and ozone; NATURAL includes solar and volcanic aerosols (events shown as green triangles on the bottom axis). Observed ocean heat content changes are shown as well. From Delworth et al., 2005.

Distinctions in the climate response do appear to arise in the vertical, where absorbing aerosols produce warming that is exhibited throughout the troposphere and into the stratosphere, whereas reflective aerosols cool the troposphere but warm the stratosphere (Hansen et al., 2005; IPCC, 2007). Delworth et al. (2005) noted that in the ocean, the cooling effect of aerosols extended to greater depths, due to the thermal instability associated with cooling the ocean surface. Hence the temperature response at levels both above and below the surface may provide an additional constraint on the magnitudes of each of these forcings, as may the difference between Northern and Southern Hemisphere changes (IPCC, 2007 Chapter 9). The profile of atmospheric temperature response will be useful to the extent that the vertical profile of aerosol absorption, an important parameter to measure, is known.

3.6.2. Implications for Climate Model Simulations

The comparisons in Sections 3.2 and 3.3 suggest that there are large differences in model calculated aerosol distributions, mainly because of the large uncertainties in modeling the aerosol atmospheric processes in addition to the uncertainties in emissions. The fact that the total optical depth is in better agreement between models than the individual components means that even

with similar optical depths, the aerosol direct forcing effect can be quite different, as shown in the AeroCom studies. Because the diversity among models and discrepancy between models and observations are much larger at the regional level than in global average, the assessment of climate response (e.g. surface temperature change) to aerosol forcing would be more accurate for global average than for regional or hemispheric differentiation. However, since aerosol forcing is much more pronounced on regional than on global scales because of the highly variable aerosol distributions, it is insufficient or even misleading to just get the global average right.

The indirect effect is strongly influenced by the aerosol concentrations, size, type, mixing state, microphysical processes, and vertical profile. As shown in previous sections, very large differences exist in those quantities even among the models having similar AOD. Moreover, modeling aerosol indirect forcing presents more challenges than direct forcing because there is so far no rigorous observational data, especially on a global scale, that one can use to test the model simulations. As seen in the comparisons of the GISS and GFDL model climate simulations for IPCC AR4, aerosol indirect forcing was so poorly constrained that it was completely ignored by one model (GFDL) but used by another (GISS) at a magnitude that is more than half of the direct forcing, in order to reproduce the observed surface temperature trends. A majority of the climate models used in IPCC AR4 do not consider indirect effects; the ones that did were mostly limited to highly simplified sulfate indirect effects (Table 3.6). Improvements must be made to at least the degree that the aerosol indirect forcing can no longer be used to mask the deficiencies in estimating the climate response to greenhouse gas and aerosol direct RF.

3.7. Outstanding Issues

Clearly there are still large gaps in assessing the aerosol impacts on climate through modeling. Major outstanding issues and prospects of improving model simulations are discussed below.

Aerosol composition: Many global models are now able to simulate major aerosol types such as sulfate, black carbon, and POM, dust, and sea salt, but only a small fraction of these models simulate nitrate aerosols or consider anthropogenic secondary organic aerosols. And it is difficult to quantify the dust emission from human activities. As a result, the IPCC AR4 estimation of the nitrate and anthropogenic dust TOA forcing was left with very large uncertainty. The next generation of global models should therefore have a more comprehensive suite of aerosol compositions with better-constrained anthropogenic sources.

Aerosol absorption: One of the most critical parameters in aerosol direct RF and aerosol impact on hydrological cycles is the aerosol absorption. Most of the absorption is from BC despite its small contribution to total aerosol load and AOD; dust too absorbs in both the short and long-wave spectral ranges, whereas POM absorbs in the UV to visible. The aerosol absorption or SSA, will have to be much better represented in the models through improving the estimates of carbonaceous and dust aerosol sources, their atmospheric distributions, and optical properties.

Aerosol indirect effects: The activation of aerosol particles into CCN depends not only on particle size but chemical composition, with the relative importance of size and composition unclear. In current aerosol-climate modeling, aerosol size distribution is generally prescribed and simulations of aerosol composition have large uncertainties. Therefore the model estimated "albedo effect" has large uncertainties. How aerosol would influence cloud lifetime/cover is still in debate. The influence of aerosols on other aspects of the climate system, such as precipitation,

is even more uncertain, as are the physical processes involved. Processes that determine aerosol size distributions, hygroscopic growth, mixing state, as well as CCN concentrations, however, are inadequately represented in most of the global models. It will also be difficult to improve the estimate of indirect effects until the models can produce more realistic cloud characteristics.

Aerosol impacts on surface radiation and atmospheric heating: Although these effects are well acknowledged to play roles in modulating atmospheric circulation and water cycle, few coherent or comprehensive modeling studies have focused on them, as compared to the efforts that have gone to assessing aerosol RF at TOA. They have not yet been addressed in the previous IPCC reports. Here, of particular importance is to improve the accuracy of aerosol absorption.

Long-term trends of aerosol: To assess the aerosol effects on climate change the long-term variations of aerosol amount and composition and how they are related to the emission trends in different regions have to be specified. Simulations of historical aerosol trends can be problematic since historical emissions of aerosols have shown large uncertainties—as information is difficult to obtain on past source types, strengths, and even locations. The IPCC AR4 simulations used several alternative aerosol emission histories, especially for BC and POM aerosols.

Climate modeling: Current aerosol simulation capabilities from CTMs have not been fully implemented in most models used in IPCC AR4 climate simulations. Instead, a majority employed simplified approaches to account for aerosol effects, to the extent that aerosol representations in the GCMs, and the resulting forcing estimates, are inadequate. The oversimplification occurs in part because the modeling complexity and computing resource would be significantly increased if the full suite of aerosols were fully coupled in the climate models.

Observational constraints: Model improvement has been hindered by a lack of comprehensive datasets that could provide multiple constraints for the key parameters simulated in the model. The extensive AOD coverage from satellite observations and AERONET measurements has helped a great deal in validating model-simulated AOD over the past decade, but further progress has been slow. Large model diversities in aerosol composition, size, vertical distribution, and mixing state are difficult to constrain, because of lack of reliable measurements with adequate spatial and temporal coverage (see Chapter 2).

Aerosol radiative forcing: Because of the large spatial and temporal differences in aerosol sources, types, emission trends, compositions, and atmospheric concentrations, anthropogenic aerosol RF has profound regional and seasonal variations. So it is an insufficient measure of aerosol RF scientific understanding, however useful, for models (or observation-derived products) to converge only on globally and annually averaged TOA RF values and accuracy. More emphasis should be placed on regional and seasonal comparisons, and on climate effects in addition to direct RF at TOA.

3.8 Conclusions

From forward modeling studies, as discussed in the IPCC (2007), the direct effect of aerosols since pre-industrial times has resulted in a negative RF of about -0.5 ± 0.4 W m^{-2}. The RF due to cloud albedo or brightness effect is estimated to be -0.7 (-1.8 to -0.3) W m^{-2}. Forcing of similar magnitude has been used in some modeling studies for the effect associated with cloud lifetime, in lieu of the cloud brightness influence. The total negative RF due to aerosols according to IPCC (2007) estimates is therefore -1.3 (-2.2 to -0.5) W m^{-2}. With the inverse approach, in which

aerosols provide forcing necessary to produce the observed temperature change, values range from -1.7 to -0.4 Wm^{-2} (IPCC, 2007). These results represent a substantial advance over previous assessments (e.g., IPCC TAR), as the forward model estimated and inverse approach required aerosol TOA forcing values are converging. However, large uncertainty ranges preclude using the forcing and temperature records to more accurately determine climate sensitivity.

There are now a few dozen models that simulate a comprehensive suite of aerosols. This is done primarily in the CTMs. Model inter-comparison studies have shown that models have merged at matching the global annual averaged AOD observed by satellite instruments, but they differ greatly in the relative amount of individual components, in vertical distributions, and in optical properties. Because of the great spatial and temporal variations of aerosol distributions, regional and seasonal diversities are much larger than that of the global annual mean. Different emissions and differences in atmospheric processes, such as transport, removal, chemistry, and aerosol microphysics, are chiefly responsible for the spread among the models. The varying component contributions then lead to differences in aerosol direct RF, as aerosol scattering and absorption properties depend on aerosol size and type. They also impact the calculated indirect RF, whose variations are further amplified by the wide range of cloud and convective parameterizations in models. Currently, the largest aerosol RF uncertainties are associated with the aerosol indirect effect.

Most climate models used for the IPCC AR4 simulations employed simplified approaches, with aerosols specified from stand-alone CTM simulations. Despite the uncertainties in aerosol RF and widely varying model climate sensitivity, the IPCC AR4 models were generally able to reproduce the observed temperature record for the past century. This is because models with lower/higher climate sensitivity generally used less/more negative aerosol forcing to offset the greenhouse gas warming. An equally good match to observed surface temperature change in the past could be obtained from a model with larger climate sensitivity and smaller net forcing, or a model with smaller sensitivity and larger forcing (Hansen et al., 2007). Obviously, both greenhouse gases and aerosol effects have to be much better quantified in future assessments.

Progress in better quantifying aerosol impacts on climate can be made only when the capabilities of both aerosol observations and models are improved. The primary concerns and issues discussed in this chapter include:

- Better representation of aerosol composition and absorption in the global models
- Improved theoretical understanding of subgrid-scale processes crucial to aerosol-cloud interactions and lifetime
- Improved aerosol microphysics and cloud parameterizations
- Better understanding of aerosol effects on surface radiation and hydrological cycles
- More focused analysis on regional and seasonal variations of aerosols
- More reliable simulations of aerosol historic long-term trends
- More sophisticated climate model simulations with coupled aerosol and cloud processes
- Enhanced satellite observations of aerosol type, SSA, vertical distributions, and aerosol radiative effect at TOA; more coordinated field experiments to provide constraints on aerosol chemical, physical, and optical properties.

A discussion of the "way forward" toward better constraints on aerosol radiative forcing, and hence climate sensitivity, is provided in the next chapter.